To the Graduate Council:

I am submitting herewith a dissertation written by Nazmul Islam entitled "AC Electroosmosis for Lab-On-a-Chip Applications" I have examined the final electronic copy of this dissertation for form and content and recommend that it be accepted in partial fulfillment of the requirements for the degree of Doctor of Philosophy, with a major in Electrical Engineering.

Jie Wu
Major Professor

We have read this dissertation and recommend its acceptance:

Samir El-Ghazaly

Syed K. Islam

Mohamed Mahfouz

Accepted for the Council:

Carolyn Hodges

Dean of Graduate School

(Original signatures are on file with official student records.)

AC ELECTROOSMOSIS FOR LAB-ON-A-CHIP APPLICATIONS

A Dissertation
Presented for the
Doctor of Philosophy Degree

The University of Tennessee, Knoxville

Nazmul Islam

May, 2007

ABSTRACT

AC electrokinetics is the study of particle and fluid motion induced by AC electric fields. In the last decade it has received increasing interest due to its important applications in micro total analysis systems and miniaturized biomedical devices. With the application of very low voltage (~1V_{rms}), AC electrokinetics can be utilized to control and manipulate particles and fluids at the micro/nano scale, which are very difficult to achieve with existing techniques, such as pressure driven flow.

Through the interaction of ac electric fields and particles/fluids, ac electrokinetics can be used to sort, separate and filter particles, and to pump and mix fluids. AC electrokinetics can operate at relatively low voltages, which is suitable for integrated lab-on-a-chip systems. This research investigates AC electroosmosis for manipulating nanofluids/ particles with an aim to provide a generic platform for the transport and concentration functions in microfluidic devices. It is envisioned that these concepts can be integrated with life science and biomedical technologies to develop a new generation of labs-on-a-chip, with high-efficiency particle manipulation and sensing, micropumps and microfluidic mixers.

Two topics are studied in this thesis. One is the trapping/concentration of colloidal and bio-particles. Particle trapping is conducted adjacent to an electrolyte/electrode interface of the gold (Au) electrode pair. We have developed the capability to integrate AC electroosmotic trap and micro-cantilever (MC) in a

microfluidic system. By combining both experimental investigation and theoretical analysis, this research work demonstrates a microcantilever particle trap.

The second topic is the transport/mixing of fluids. An original biased AC electroosmotic pump is being developed, and experiments have been performed to prove the concept. Both numerical simulation and pumping experiment is done to optimize the pumping efficiency. The control of the biased AC-EO pumping is also suggested by using the feedback loop.

The thesis concludes with suggestions on how the concepts can be exploited for the development of new strategies for colloidal separation, manipulation for microfluidics and bioMEMS technologies.

ACKNOWLEDGMENTS

I am most grateful to my advisor Dr. Jie (Jayne) Wu for all the help and guidance she has provided me throughout my Ph.D. study. This work would have never been completed without her guidance.

Many thanks to Dr. Syed K. Islam to support me to start my Ph.D. program and helped me to work with Life Science Division at ORNL. He also inspired me a lot with good suggestions.

I would like to extend my gratitude to Dr. Samir El-Ghazaly and Dr. Mohamed Mahfouz for undertaking the extra effort to serve on my Ph.D. committee. Especially to Dr. El-Ghazali who gave me some invaluable advice of my future goals, research and career development.

I would like to thank sincerely to the faculty and staff of Electrical and Computer Engineering Department for their part in my graduate educational development. Special thanks to Dr. Bouldin for his invaluable suggestions. I am grateful to CNMS group members of ORNL, especially Dale Hensley, Richard Kasica, Ruby Farahi and Darrel Thomas for their help on the cleanroom usage. I would also like to thank Dr. David Joy for helping me with electron microscopic facility and Tom Malmgren for help on atomic force microscope.

Special thanks go to our Electromechanics and Transducer Research Group members, James Wilson, Meng Lian, Kai Yang, Sangeetha Swaminathan, Jayanth

Kruttiventi, and Prachya Mruetusatorn, for creating an educational and friendly environment inside the group.

Finally, I would like to express my deepest gratitude to my parents, wife and daughter for their endless love, support and encouragement.

TABLE OF CONTENTS

LIST OF FIGURES

Figure Page

ABBREVIATION AND ACRONYMS

AC	Alternating Current
ACEO	AC Electro-osmosis
AFM	Atomic Force Microscopy
AP-ACEO	Asymmetric Polarization ACEO
DC	Direct Current
DEP	Di-Electrophoresis
DI	Deionised
EK	Electro-kinetic
EOF	Electroosmosis Flow
ET	Electro Thermal
FL	Fluorescent
ITO	Indium Titanium Oxide
LOC	Lab-On-a-Chip
MC	Micro-cantilever
MEMS	Microelectromechanical systems
PDMS	Poly-dimethyl-siloxane
PECVD	Plasma enhanced Chemical Vapor Deposition
PS	Poly-sterine
RIE	Reactive Ion Etching
SEM	Scanning Electron Microscopy
μTAS	Micro Total Analysis and System

CHAPTER 1. INTRODUCTION

1.1. INTRODUCTION

Micro-/Nano- fluid devices are becoming more prevalent, both in commercial applications and in scientific inquiry. Microfluidics is a key enabling factor in the miniaturization and integration of multiple functionalities for chemical analysis and synthesis in handheld microdevices, which require efficient methods for manipulating ultra small volumes of liquid as well as the contents in the fluid within the fluid networks. For biomedical applications, microfluidic chip arrays are being used to identify multiple bioparticles [1]. Recent developments in micro-fabrication technologies enabled different types of microfluidic functions such as micro-pumps [2, 3], micro-mixers [4], particle concentrator [5,6], and various types of injection systems (nano-needles).

At the very beginning of microfluidics, people thought that microfluidic devices could just be a miniaturized version of macro- fluidic devices. The technological advancement on microfluidic systems has proven that the problem is far more complicated than scaling down a device geometrically. Therefore, a better understanding of the micro/nano scale properties is in order. A dominant difference of microfluidic devices from their macro-scale counterparts is the increased surface/volume ratio, hence dominant surface force effects/friction.

For example, micro channel needs high pressure for pressure driven flow to produce sufficient flow rate. The formula below relates the applied pressure with the conduit radius for a constant flow rate.

$$\Delta P = \frac{8\mu L Q}{\pi a^4} \qquad \mu : \text{viscosity};\ a : \text{conduit radius}$$

Every time we try to reduce the conduit radius into half, we need to have sixteen times of larger pressure to sustain the same flow rate. So at microscale, surface forces start to dominate due to the large surface/volume ratio. Therefore electroosmosis (as a type of surface forces) becomes the prime candidates for fluidic manipulation at micro scale.

DC electroosmosis (DC EO) has a long history of being applied in miniaturized biochemical devices. However, DC EO has many undesirable effects, such as high voltage operation, electrolysis and resulting bubble generation, and pH gradient. In this thesis, we examined a new type of EO phenomena, ACEO, and how it can be employed to integrate with the microcantilever particle trapping.

1.2. MICROFLUIDICS: PAST, PRESENT AND FUTURE

Microfluidics is an interdisciplinary area that focuses on the miniaturization of fluid-handling systems. The concept of complete lab-on-a-chip devices or micro-total analysis systems (μ-TAS), has recently generated great interest in a variety of industries, where transport and processes (including mixing, reaction, separation, and manipulation of chemicals and particles) are being applied on much smaller scales than traditional

engineering technologies [8]. This interest has led to tremendous growth in microfluidic technologies over the past decade.

A functional microfluidic chip should be able to realize certain functions, such as transporting, mixing (with reactants), sample treatment (concentrating, sorting). Figure 1-1 gives an example of a generic microfluidic chip.

Unlike the microelectronics industry, where the current emphasis is on reducing the size of transistors, the field of microfluidics is focusing on investigating new fluid phenomenon at micro/nano-scale with more sophisticated fluid-handling capabilities. One of the promising types of micropumps is driven by electroosmosis (EO). EO pumps are purely driven by electric fields and have no moving parts. In general by EO pump we understand the DC-EO pump. If the channel length of the DC-EO pump is high, it requires very high voltage (~kV) for pumping action. The central concept of micro/nano-scale fluid transportation is utilizing the surface force. As the surface to volume ratio of the microchannel is high, the dominant surface force is a good choice for pumping the liquid in microchannel. As mentioned before, the field of microfluidics has far more complexity than people first expected. The dominant/efficient mechanism to manipulate fluid or biochemical samples will change with sample conductivity, pH value, and sample sizes. Also, we need to be concerned with side effects from those actuation mechanisms. So microfluidic industry did not develop in a similar way as the microelectronics industry. But in recent years the lab-on-a-chip (LOC) devices are getting sufficient attention for various applications.

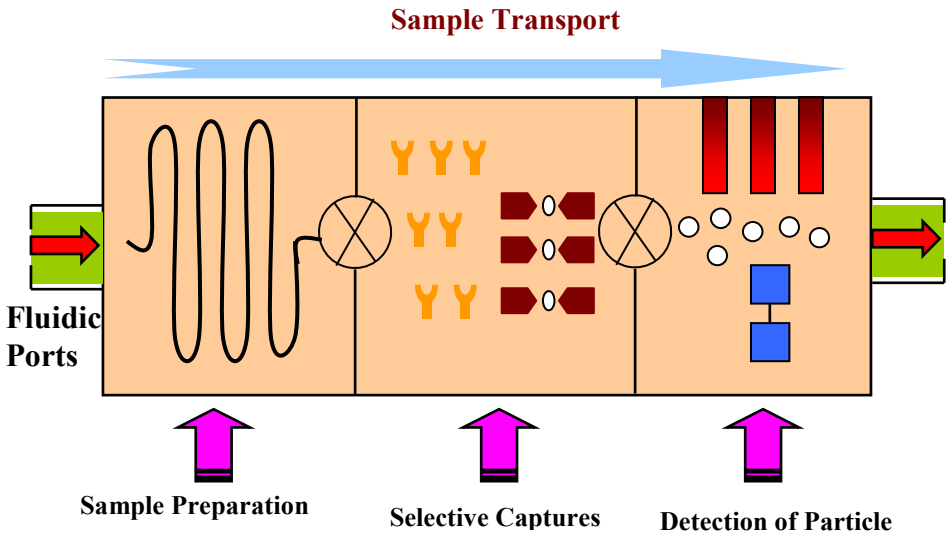

Fig. 1-2. A Generic Microfluidic Chip

Lab-on-a-chip devices have shown commercial success in biological applications such as electrophoretic separations and DNA sequencing, where DC electrokinetics or DC electric field is used to manipulate fluid/particles (here surface force is used versus pressure driven). However, because of its operation with high voltage, there are obstacles to extend DC electrokinetics to more fluidic functions. On the other hand, AC electrokinetics has important potentials in the field of life science. With the capability to manipulate particle and fluid motion at the microscale with low voltage, it meshes well with the requirements of lab-on-a-chip systems.

My research is a combination of sample transportation and particle detection in a microfluidic chip. As shown in figure 1-1, we need to transport the sample, for which I have experimentally validate the biased ACEO micro-pumping. The developed micropump is operated with smaller AC voltage, which is compatible with the lab-on-a-chip. For particle detection as shown in figure 1-1, we need high effective techniques to detect micro/nano-scale particulate. We also have envisioned to develop the validation technique for particle trapping. That is the reason we have interface the microcantilever with our microfluidic device. The applications of this integration can greatly benefit the advancement of AC electrokinetics.

1.3. ELECTROKINETICS

Electrokinetics is the combination of “electric” plus “kinetics”. Generally speaking, electrokinetics is the motion of liquid or particle under the influence of electric field. According to Probstein [7], the electrokinetic effects have been first observed by F.

F. Reuss in 1809 via experiments on porous clay diaphragms. He has shown that in capillary, fluid moves from anode to cathode in the presence of an external electric field. In the mid 19^{th} century, Wiedemann repeated this experiment and described the fundamentals of electrokinetics. This was followed later by the seminal work of Helmholtz in 1879 on the electric double layer theory, which related the electrical and flow parameters for electrokinetic transport.

DC electrokinetics, including electroosmosis and electrophoresis, has almost two hundreds years' history and has been rather thoroughly investigated. Electroosmosis is the fluid motion caused by the electrical force acting on the double layers next to a charge surface. The ions in a double layer are moved by a tangential electric field, giving rise to movement of the whole double layer along the surface, which in turn puts the bulk fluid into motion through the viscous interaction.

On the other hand, AC electrokinetics has been studied for just a few years. AC electrokinetics can be classified into three categories, dielectrophoresis (DEP), the electrothermal effect (ET) and ac electroosmosis (ACEO). DEP is the force acting on the particles due to the difference in polarizability between the particles and the fluid. The electrothermal effect refers to the fluid motion caused by the interaction of electric fields and gradients of conductivity and permittivity of the fluid through Joule heating. AC electroosmosis is the fluid motion induced by moving double layers. We will focus on the AC electroosmosis, while we will discuss the effects from other electrokinetic phenomena.

Basically, AC electroosmosis (ACEO) works by the same principle as DC EO. However, in ACEO, the surface charges are induced by externally applied voltages, rather than naturally occurring charges in DCEO, and consequently hundreds of time stronger. As a result, ACEO can generate flow velocity of several hundreds microns per second with a couple of volts.

AC techniques are more favorable over DC ones for following reasons: (1) low operating voltage makes it superior in terms of device portability; (2) avoids electrolysis and the resulting bubble generation; (3) minimizes pH gradient; (4) miniaturization and integration with other devices on lab-chips.

We have extended the scope of ACEO by including electrochemical reactions (i.e. Faradaic charging), and then developed a new ACEO technique—asymmetric polarization ACEO. Asymmetric polarization of electrodes is achieved by combining the DC bias into AC signals over electrode pairs. Biased ACEO breaks the reflection symmetry to produce net flow in a symmetric pair of electrode. This technique adds more flexibility to the faster manipulation of bio-particulate .

1.4. THESIS ORGANIZATION

Chapter 2 will first give the literature review on electroosmosis and governing equation of electrical double layer (EDL) theory. Then microfluidic electrokinetics is reviewed. The fabrication process of microfluidic devices is also presented in this chapter. Chapter 3 describes the AC electroosmosis particle trapping by the interdigitated electrode pattern

with both symmetric and asymmetric electric signals. Electric field simulation was performed to understand the interplay between the electric fields and induced surface charge in electrolytes, which forms AC electroosmosis. In Chapter 4 we discuss the parallel plate particle trapping, which is the basis of our new cantilever particle trapping. Here we present a first ever particle trap on microcantilever. Its trapping effect is validated using multimode AFM. The particle trapping configuration was also verified using the scanning electron microscope (SEM). Initial thoughts and design on asymmetric polarization ACEO are included in chapter 5. The experimental and simulation result of the biased ACEO is also presented in this chapter. Finally, the conclusion and future work is presented in Chapter 6.

CHAPTER 2. LITERATURE REVIEW

2.1. INTERFACIAL CHARGING AND ELECTROOSMOSIS

Electroosmosis (EO) is used for microscale fluid manipulation and transportation. This is because the surface to volume ratio increases as the size goes down and surface force dominates. EO is a kind of surface force which originates from the charge of solid/liquid interface. The surface acquires a negative charge with contact with the fluid. This charge creates an electrostatic surface potential. By modifying the electrostatic surface potential the charges can be induced at solid/liquid interface, which in turn can manipulate fluid transport in micro/nano-scale.

2.1.1. Characteristic of Microfluidics

Microfluidics refers to the handling of fluids at a scale generally below 1 mm, where a number of phenomena that are not present or not predominant at larger scales can be exploited for numerous purposes. Microfluidics deal with the nanoliters of solution volume, micrometers of dimension, and milliseconds of diffusion and reaction time. The accurate sampling, positioning, and transport of nanoliter volumes of liquids can be possible with microfluidic devices.

As it is mentioned earlier, surface play a very important role in microfluidics. On the other hand, the large surface-to-volume ratios of microchannels can make interfacial

reactions efficient. But surface produces friction for fluid movement so, for liquid-handling methods or pumping action it is necessary to overcome the hydraulic resistance of micrometer-sized conduits. Similarly, the flow of liquids in microchannel is laminar, and therefore mixing at the micrometer scale can, in fact, be difficult to achieve. A functional microfluidic system comprise of a rich mix of elements and functionalities. It should be able to meter liquids as well as for process and analyze complex biological specimens.

The heart of a microfluidic device is often a microchannel, in which reaction, separation, or detection takes place. For this reason, thorough work has been done on optimizing the geometry of microchannels to improve their hydrodynamic properties together with fluid velocity [9-12]. There are dimensionless numbers which characterize the fluid flow in the microfluidic channel. These dimensionless numbers (Reynolds, Peclet etc.) will also be studied to understand the effects of fluid flow in micro-channel.

An important characteristic of microfluidics is the laminar flow condition. A measure of the laminar or turbulent properties of liquid flow is the Reynolds number *Re*. The Reynolds number is a measure of the relative importance of intertial to viscous terms. The Reynolds number is defined as,

$$\mathrm{Re} = \frac{\rho v_s L}{\mu} = \frac{v_s L}{v} = \frac{InertialForces}{ViscousForces}$$

where: v_s - fluid velocity,

L - characteristic length,

μ - dynamic fluid viscosity,

ν - kinematic fluid viscosity: ν = μ / ρ,

ρ - fluid density.

Reynold number characterizes the behavior of flow in general. The higher the Reynolds number, the more likely to be turbulent the flow, and the lower the number, the more likely the flow will be laminar. In microfluidic experiments Reynold number is typically much lower than 2000. By assuming the fluid velocity of 300 μm/sec and characteristic length 50 micron, the Reynold number for our microfluidic system is around 15, which is very small in number. For this small Reynold number the viscous force dominates in our analysis.

Another important parameter of the microfluidic is the Peclet number, which characterizes the mixing of the liquid. The Peclet number (Pe) is a measure of the relative importance of advection to diffusion. The higher the Peclet number, the more important is advection.

$$Pe = \frac{lv}{\alpha}$$

where, l = Characterisitic length

v = Velocity

α = Thermal Diffusivity

From the equation of Peclet number we can see that for smaller mixing length (l) the Peclet number will be smaller. If we get smaller Peclet number for a mixing system then the time of mixing is smaller. Peclet number range between 10^1 and 10^5, also

indicated that convection is much faster than molecular diffusion [13]. By assuming the velocity 300 μm/sec and the characteristic length of 50 micron, for our experimental setup, the calculated Peclet number is 150 (Thermal diffusivity = 10^{-2} cm^2sec^{-1}). So for this Peclet number the pumping is happened, which supersede the diffusion affect. Due to the large surface to volume ratio in microchannels, surface tension and viscous forces play a considerable role in the flow characteristics, which we will discuss more in the latter chapters.

2.1.2. Electroosmosis

Electroosmosis is the motion of liquid through a membrane / porous material under the influence of an applied electric field. The direction and flow rate of electroosmotic flow is determined by many factors, such as the electric field strength, the concentration of electrolytes, the surface charge density on the inner surface of the channel or capillary, temperature, pressure, viscosity etc.

A typical electroosmotic flow system is shown in Fig. 2-1. The interface between solid/electrolyte is typically negatively charged. The surface charge is positive or neutral for some materials and the polarity and intensity of the surface charge depends on the material and the environment such as pH and temperature. In the case shown in Fig. 2-1, counter-ions (ions have opposite charges to the surface) are cations, and co-ions (ions have same charges as the surface) are anions. Anions are expelled away from the surface by the negative surface charges, while cations are attracted to the surface. Therefore, cations are adsorbed and accumulate on the inner surface of the channel, while anions are

driven out of this region. Usually, the strongly adsorbed cations cannot fully offset the surface charges, so there are some loosely adsorbed cations exist outside them, and the total surface charge is fully balanced by the cations at certain distance. For channels having negatively charges on surfaces, the solution inside the channel flows toward the cathode, (because of viscosity) which is known as (DC) electroosmosis. The velocity profile of a fully developed electroosmotic flow (EOF) in channels with thin EDL is shown in figure 2-1. Figure 2-2 also shows the concentration difference between counterions and coions near the interface.

2.2. CLASSICAL ELECTRICAL DOUBLE LAYER (DBL) THEORIES

The double layer theory explains the evolution of double layer at the solid-liquid interfaces and introduces the electroosmotic force in the electrolyte. This section will analyze the double layer theory, which will calculate the double layer thickness. It is also possible to calculate the zeta potential from the value of double layer thickness. The analysis of double layer can relate the concentration of surface ions on the interface, which will also denote the strength of AC electroosmosis (ACEO). First, let us derive the relationship between the electrolyte properties and the development of DBL, such as its thickness and charge density.

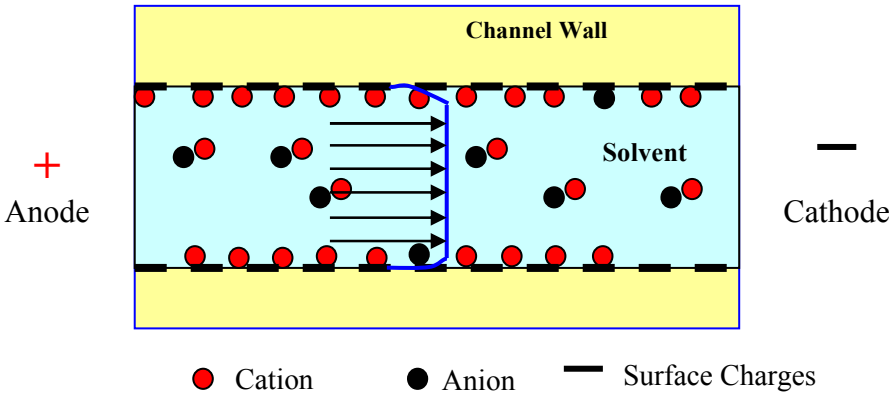

Fig. 2-1. DC electroosmotic flow in a negatively charged channel with thin EDL. Instead of showing directly as molecules, the solvent are represent by the yellowish colored area.

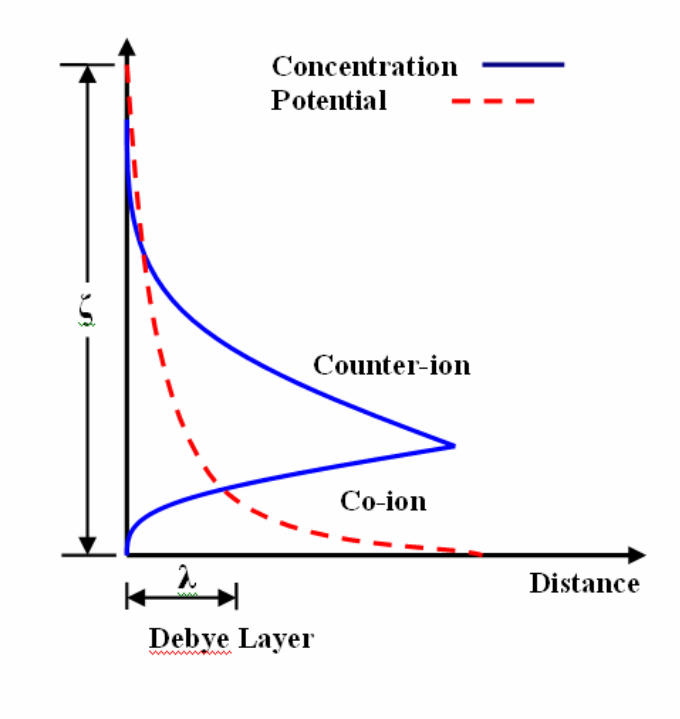

Fig. 2-2. Plot of electrolyte concentration with respect to distance in the bulk; Boltzmann distribution of ions.

At electrochemical equilibrium, the density of electrolyte *i* follows a Boltzmann distribution:

$$\rho_i\left(r^*\right) = \rho_i^0 e^{\frac{-z_i e\phi^*\left(r^*\right)}{kT}} \tag{2-1}$$

where, $r^*(x^*, y^*, z^*)$ is the vector in Cartesian coordinates,

ϕ^* is the electrical potential in Volts,

z_i is the valence of ion species i,

e is the elementary charge (or electron charges),

k is the Boltzman constant,

T is the absolute temperature in kelvins, and

ρ_i^0 is the number density (i.e. numbers per cube meter) of ion species *i* a the location where $\phi^* = 0$.

According to Poisson's equation,

$$\nabla^2\phi^*\left(r^*\right) = -\frac{1}{\varepsilon_r\varepsilon_0}\rho_e\left(r^*\right) = -\frac{1}{\varepsilon_r\varepsilon_0}e\sum_i z_i\rho_i\left(r^*\right) \tag{2-2}$$

where ε_r is the dielectric constant of the substance, and

ε_0 is the permittivity of free space

Combining the above two equations, we get

$$\nabla^2\phi^*\left(r^*\right) = -\frac{1}{\varepsilon_r\varepsilon_0}e\sum_i z_i\rho_i^0 e^{-\frac{z_i e\phi^*\left(r^*\right)}{kT}} \tag{2-3}$$

which is well-known as Poisson-Boltzmann equation.

For cases where the Debye-Huckel limit $\left|\frac{z_i e\phi^{*0}}{kT}\right| << 1$ is satisfied, we have $\left|\frac{z_i e\phi^{*}}{kT}\right| << 1$, since $\phi^{*0} \le \phi^{*} \le 0$. Using Taylor series, noticing that $\sum_i z_i \rho_i^0 = 0$, because the solution is electrically neutral and equation (2-3) can be simplified to,

$$\begin{aligned} \nabla^2 \phi^*\left(r^*\right) &= -\frac{1}{\varepsilon_r \varepsilon_0} e \sum_i z_i \rho_i^0 \left(1 - \frac{z_i e \phi^*(r^*)}{kT}\right) \\ &= \sum_i \frac{z_i^2 e^2 \rho_i^0 \phi^*(r^*)}{\varepsilon_r \varepsilon_0 kT} \end{aligned} \tag{2-4}$$

and from $\frac{z^0 e\phi^*(r^*)}{kT} << 1$, we have $\phi^* << 0.026$ volts.

Now we define the potential scale $\phi_0 = \frac{kT}{e} = \frac{RT}{F}$, and nondimensionalizing equation (2-4) with $\phi\left(r(x,y,z)\right) = \frac{\phi^*\left(r^*\right)}{\phi_0}, x = \frac{x^*}{L}, y = \frac{y^*}{h}, z = \frac{z^*}{W}$, where L, h and W are the length height and the width of the channel. Now we get,

$$\varepsilon_1^2 \frac{\partial^2 \phi}{\partial x^2} + \frac{\partial^2 \phi}{\partial y^2} + \varepsilon_2^2 \frac{\partial^2 \phi}{\partial z^2} = h^2 \kappa^2 \phi \tag{2-5}$$

where, $\kappa = \sqrt{\frac{\sum_i z_i^2 \rho_i^0 e^2}{\varepsilon_r \varepsilon_0 kT}}, \varepsilon_1 = \frac{h}{L}, \varepsilon_2 = \frac{h}{W}$.

The reciprocal of κ has dimension of length. Thus it is a characteristic thickness of the electric double layer (EDL).

From κ we defined EDL thickness, or Debye length, λ, as

$$\lambda = \frac{1}{\kappa} = \sqrt{\frac{\varepsilon_r \varepsilon_0 kT}{e^2 \sum_i z_i^2 \rho_i^0}} = \sqrt{\frac{\varepsilon_r \varepsilon_0 kT}{2z^2 q^2 n_0}} \tag{2-6}$$

The thickness of the diffuse double layer generally ranges from several to few hundred nanometers, depending upon bulk ionic concentration and other physicochemical properties of liquid. It depends solely on the properties of electrolytes, no dependence on the solid properties.

As an example, if we want to calculate the Debye length of glass/water interface, we need to calculate n_0 first. Debye length generally depends on the concentration.

$$n_0 = 10^{-7} mol/l \times 1000 l/m^3 \times 6.023e^{23} / mol = 6.023e^{19} / m^3$$

By putting all the values in eqn. (2-6) we get debye length is 961.542 nm.

The electrical static potential at the surface is termed as zeta potential, ζ, which is dependent on the surface material. Using Debye-Huckel approximation, the zeta potential across the double layer can be calculated by, $\varsigma = \frac{\sigma\lambda}{\varepsilon}$

2.3. ELECTROOSMOSIS FLUID FLOW

Figure 2-3 is illustrating the geometry of the theoretical model. The x and y axis is shown in the figure. Fluid motion in the double layer is governed by,

$$\rho_m \frac{D\vec{u}}{Dt} = -\nabla p + \mu \nabla^2 \vec{u} + \rho \vec{E} \tag{2.7}$$

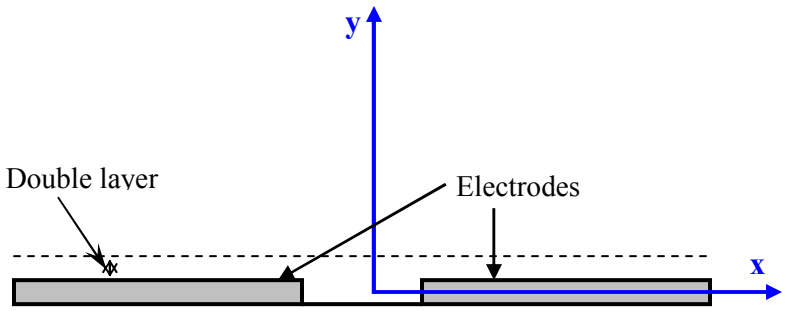

Fig. 2-3. Schematic illustrating the geometry used in the theoretical model

Assuming that the Reynold's number is sufficiently small so that the term on the left hand side is negligible, and the pressure and the velocity remain the same along x-direction (Fig. 2.3), equation (2.7) is simplified to,

$$\mu \frac{\partial^2 u}{\partial y^2} = -\rho E_x \tag{2.8}$$

where u is the fluid velocity at x-direction. Combining with the Gauss's law gives,

$$\mu \frac{\partial^2 u}{\partial y^2} = \varepsilon \frac{\partial^2 \phi}{\partial y^2} E_x \tag{2.9}$$

Integrating this equation twice and applying the boundary conditions,

$$\begin{aligned} &\phi = \zeta \quad \text{at} \quad u = 0 \\ &\frac{\partial u}{\partial y} = \frac{\partial \phi}{\partial y} = 0 \quad \text{as} \quad y \to \infty \end{aligned} \tag{2.10}$$

We obtain, the fluid motion,

$$u_x = -\frac{\varepsilon}{\mu} \zeta E_x \tag{2.11}$$

This equation is known as Smoluchowski's 'slip velocity'.

For applying an electrical signal on the charged surface, the electric field will exert a force on the diffuse layer. This diffuse layer is a part of the fluid, and the migration of the mobile ions will drag the fluid with them (Fig. 2-1). Where E_x is the electric field tangential to the charged surface and μ is the viscosity. This can be interpreted as the slip velocity and is linearly proportional to tangential electric field E_x, charge density in DBL, ζ, that is available to propel the fluid, and inversely proportional to the fluid viscosity, μ, that is retarding the flow (equation 2.11).

2.4. THEORY OF AC ELECTROKINETICS

AC electrokinetics provides a means to effectively control and manipulate particles and fluids at micro-scale. Switching electric field of AC elctrokinetics can suppress the electrolysis and hence the change of pH value at electrodes, which is inevitable in dc electrokinetics. Different from DC EO which relies on naturally induced charges, ACEO induces surface charges by applying voltage, which can be hundreds of times higher lower voltage is required to generate sufficient flow velocity. Additionally small spacing of electrodes makes it possible to reach high electric field (E) with low applied voltage (V). AC electrokinetics can operate low voltages, which is suitable for lab-on-a-chip operation.

AC electrokinetics comprises of dielectrophoresis, the thermal effect and ac electroosmosis. Dielectrophoresis (DEP) is the response of particles to the applied electric fields, and the electrothermal effect and ac electroosmosis are fluid motion caused by AC fields.

Ramos et al have provided a rather comprehensive review [9] on various forces acting on micro-size particles on microelectrode arrays when electrodes are energized with ac voltages over a wide range of frequency. In subsequent work, Ramos et al [10] presented a RC model describing the frequency dependence of ACEO flow velocity by capacitive charging of the electrodes. Recently, Bazant and Squires [25, 30] also presented that AC electrokinetic phenomena can also occur for conducting particles, which they termed as Induced charged Electroosmosis (ICEO). They also predict that the velocity will scale as E^2, where E is the applied electric field. Vortices will also occur around a spherical metal because of their geometry. Bhatt [5] also reported that electrohydrodynamic effect arising from the application of alternating electric fields to patterned electrode surfaces. Olesen [31] also have demonstrated that AC electrokinetic (more specific AC EO) micropumps permit integrable, local, and fast pumping (velocities » mm/s) with low driving voltage of a few volts and asymmetric electrode pattern.

2.4.1. AC Electroosmosis

AC electroosmosis is induced by ac electric fields, which provides not only the tangential component of electric field but also the surface charge. The interaction of this tangential electric field with the surface charge produces the counter rotating vortices, which introduce the fluid flow on the surface.

Similar to DC electroosmosis, AC electroosmosis drives the bulk fluid through the interaction of double layers and external electric fields [9, 10, 22, 34, 42]. While DC electroosmosis has found important applications in biotechnology [18, 33], their high

voltage operation put serious limitations on their applications. So an alternative is being sought after. AC electroosmosis requires much lower voltage and simpler system structure. Operating at relatively high frequencies also helps to eliminate the electrolysis. These advantages can be used to develop new techniques for biomedical process. In the next section, theoretical study of AC electroosmosis is presented.

2.4.2. Dielectrophoresis

Dielectrophoresis refers to the force exerted on an uncharged particle in aqueous medium induced by nonuniform electric fields. The efficiency of this method depends on how polarized the particles are when compared to the fluid medium. It is of great interest in recent years because it has important potentials in separating, sorting, and filtering bioparticles, such as cell viruses, bacteria, DNA and proteins. Following are the features of DEP, which enables selective control on micro/nano-sized particles:

- The magnitude of DEP force is expressed as:

$$\langle F_{DEP} \rangle = \pi \varepsilon_m a^3 \,\mathrm{Re}\left[\frac{\tilde{\varepsilon}_p - \tilde{\varepsilon}_m}{\tilde{\varepsilon}_p + 2\tilde{\varepsilon}_m}\right] \nabla \left|E^2\right|$$

where, a is the particle diameter, ε_p is the particle permittivity, and ε_m is the permittivity of the suspending medium. The magnitude of the force also depends on the permittivity of the suspending medium. In the case of E denoted by a point charge.

$$E \propto \frac{1}{r}, \quad \nabla\left|E^2\right| \propto \frac{1}{r^3}$$

- Two kinds of DEP can take place, which we can understand from the term $\left[\frac{\tilde{\varepsilon}_p - \tilde{\varepsilon}_m}{\tilde{\varepsilon}_p + 2\tilde{\varepsilon}_m}\right]$. The positive DEP and negative DEP, depends on the sign of its polarization. Positive DEP can move particles to the high field, and negative DEP directs the particle to the low field.

As DEP is inversely proportional to the cube of characteristic length, it diminishes rapidly with the distance to surface increases. And it is not very effective manipulating particles smaller than a few microns in diameter (for a^3 term in the equation). These two properties make DEP less competitive on the particle manipulation in the bulk of fluid.

2.4.3. The Electrothermal Effect

The electric field heats the electrolyte of conductivity σ, giving the time-averaged power density dissipated in the system [20],

$$\langle P \rangle = \frac{1}{2}\left(\sigma E.E^*\right) = \frac{2}{\pi^2}\frac{\sigma V_0^2}{r^2}$$

If E is nonuniform, the power density will be nonuniform and therefore the temperature field will be nonuniform. Because conductivity and permittivity are functions of temperature, the spatially varying temperature field causes local changes of these electrical properties. The electric field interacts with the gradients of conductivity and permittivity, giving rise to the electrothermal (ET) force, which can put the fluid into motion. Electrothermal force produces fluid motion. The motion can be transferred to the

particles embedded within the fluid, causing the particles to move. So there is no dependency on particle properties.

Electrothermally-generated fluid motion is investigated experimentally and numerically in [43, 44]. Electrothermal forces become more dominant than AC electroosmosis for generation of fluid motion in high conductivity (σ = 0.66 S m^{-1}) buffers. ET has been utilized to generate micro-stirring to improve binding rates for flow-through assays [43]. However, more application of ET are yet to be explored.

2.5. Fluid Flow by AC Electroosmosis

AC electroosmosis is much more complicated than DC electroosmosis due to two reasons: 1) The applied signal is oscillating; 2) The surface charge and the tangential field are coupled. An excellent experiment and theoretical study of AC electroosmosis can be found in [9, 10, 42]

The governing equations for the fluid motion inside the double layer are still equqation (2.7) coupled with the continuity equation. Neglecting the term on the left hand side of equation (2.7) leads to,

$$-\nabla p + \mu\nabla^2 \vec{u} + \rho \vec{E} = 0 \tag{2.12}$$

The fluid velocity can be obtained after substituting the charge density (ρ) and the electric field distribution into equation (2.12). The fluid velocity at the outer boundary of the double layer is given by [42],

$$\vec{u}_f = -\frac{\varepsilon}{4\mu}\Lambda\nabla_s\left(\left|\Delta V\right|^2\right) \tag{2.13}$$

where Λ is a factor of the double layer structure, ∇_s represents a gradient across the surface, and ΔV is the potential drop across the double layer. According to the equation (2.13), fluid tends to move from higher electric field region to the lower electric field region. The fluid velocity at the electrode surface is [10],

$$u_s = \frac{1}{8}\frac{\varepsilon V_0 \Omega^2}{\mu s\left(1+\Omega^2\right)^2}, \tag{2.14}$$

where V_0 is the voltage amplitude and s is the distance from the electrode center. Ω is the nondimensional frequency,

$$\Omega = \omega\frac{\varepsilon}{\sigma}\frac{\pi}{2}\frac{s}{\lambda}, \tag{2.15}$$

where ω is the angular frequency and λ is the debye length.

Equation (2.14) gives a bell-shaped velocity profile with respect to the frequency. At high and low frequencies the velocity approaches to zero. We experimentally verified this bell-shaped velocity profile in the latter chapter.

Our research emphasizes on the charging processes of electrodes. By studying surface EO flows with respect to AC potential, we identified ACEO induced by electrochemical reactions (i.e. Faradaic charging), and we have developed a new ACEO technique — asymmetric polarization ACEO. Here we also explain the competition between the Faradaic and Capacitive charging process.

Faradaic charging generates co-ions from electrochemical reactions. When the electrode is positively charged, it goes through the reaction according to the Faradaic's

law. On the other hand, capacitive charging attracts counter-ions from the electrolyte to screen the electrode potential.

Our contribution in this field is that we have developed an "asymmetric polarization (A-P) ACEO" technique by adding a DC offset to the AC signal, and we used this A-P ACEO for trapping particles on the electrodes [11]. Asymmetric polarization of electrodes in a pair is achieved by combining the DC bias into AC signals over electrode pairs. For adding DC bias the reflection symmetry of electrode charging is broken, leading to asymmetric surface flow and net-flow. By adjusting the amplitude and frequency of AC signals, a variety of directed surface flows are produced on electrodes to manipulate and transport particles.

Capacitive charging and Faradaic charging coexist and compete for dominance when the electrodes are energized under biased conditions. The biased ACEO scheme is built on the fact that the two electrodes in a pair undergo the two distinct polarization processes. Biased AC EO is implemented by energizing electrode pairs with biased AC signals so that electrodes in a pair undergo polarizations different from each other. The advantage of such a scheme is twofold. First, it breaks the mirror symmetry of electric fields and, consequently, that of surface flows. If Faradaic charging occurs on one electrode while capacitive charging takes place on the other, then ions of the same sign populate the electrode surface and they migrate in the same direction under the influence of the electric fields. As a result, a unidirectional flow is produced at the electrode surface. So, non-uniform electric field has a good application in pumping action.

2.6. FABRICATION OF MICROFLUIDIC DEVICES

The processes developed for microelectronics, such as standard photolithographic methods, can be applied to silicon and glass substrates producing channel networks in two dimensions for sample transport, mixing, separation, and detection systems on a monolithic chip (Fig 1-1). A mask is made that has transparent and opaque regions that are patterned as a negative image of the desired channel layout. A UV-light source transfers the layout from the mask to the photoresist, which has been previously deposited on the substrate by spin-coating. The photoresist is then developed in a solvent that selectively removes either the exposed or the unexposed regions.

After developing the photoresist, it has a small amount of "hydrocarbon" material still on the wafer. If this is not removed it can affect the geomarty. Removing this very thin layer is something we call "descum". To descum we used an oxygen plasma generated in a parallel-plate etcher (Reactive Ion Etching – RIE). The oxygen plasma interacts with our undesirable hydrocarbon layer and burns it away.

Then we deposit gold using the E-beam evaporator. As an adhesive layer we have used Cromium (Cr) between the gold and the wafer. After that photoresist is removed by lift-off process, and interdigitated electrode pattern is created for microfluidic experiment. Typical fabrication sequence is shown in the figure 2-4. Here we have shown the negative photolithography, where the image reversal is used.

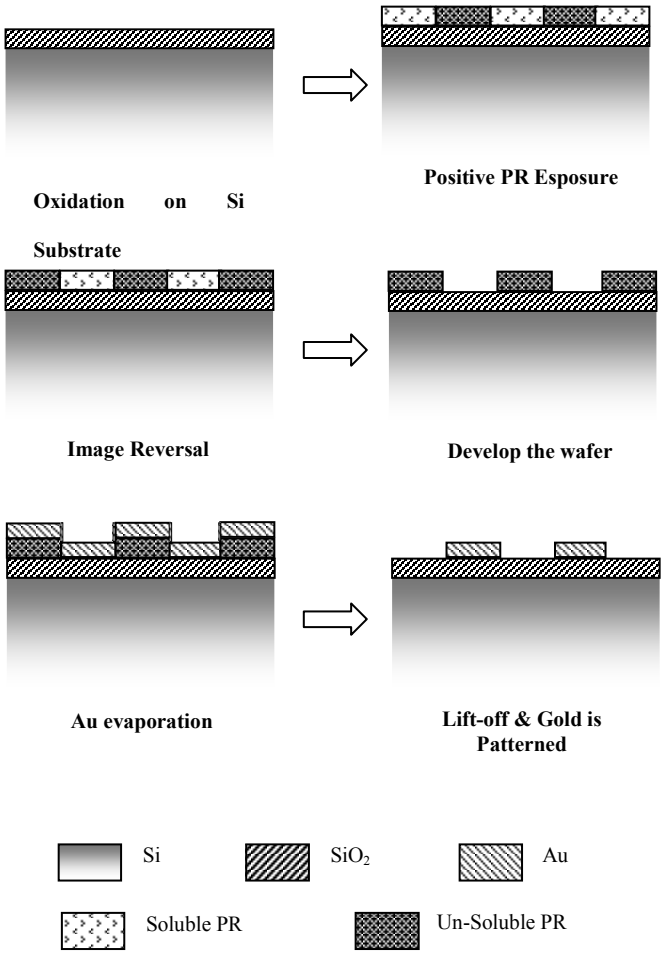

Fig. 2-4. Typical fabrication sequence for silicon, and glass microfluidic devices

Polymer based microfluidic devices are also getting much attention recent days. Polymer is resistant to chemicals and some are biocompatible for implantation by FDA [37]. PDMS has shown a number of advantages over other polymer materials (eg. SU-8, PMMA): PDMS microchips can be easily replicated and produced by rapid prototype approaches with low cost [39]. The excellent optical transparency of PDMS has been exploited to integrate different elements in the optical detection.

For our experimental we have used PDMS to fabricate our microchannel for microfluidics particle trapping and micropumping. The first step of fabricating microchannel is to have the mold. We have fabricated the channel dimensions as low as 100 μm X 100 μm [cross-section]. Following is the steps of fabricating microchannel for our experiments.

1. PDMS was prepared by thoroughly mixing the silicone Base and Curing Agent (SYLGARD 184 Silicone Elastomer Kit, Dow Corning, Midland, MI) at ratio 10:1 base:curing agent using a portable mixer. The mixture was then set in a small plastic container to reduce the air bubbles from the mixing process. This was done in approximately 30 minutes or until there were no visible bubbles. The PDMS was then poured onto two different glass substrates (microscope glass slides). The first substrate functioned as the bottom layer, which was patterned using a piece of masking tape. The pattern defined the profile of the microfluidic pump. It contained a microchannel that connected two reservoirs at the end of the channel. The second substrate created the top layer, which would be used as the channel

sealer. (See Figure 2-5a). Both substrates were thermally cured on a hot plate for 10 minutes at 150°C.

2. The PDMS for the top layer was then peeled from the glass substrate and was placed on top of the PDMS for the bottom layer. A careful placement was done to avoid any air gap between the two layers. Hence, to prevent a leak of the working liquid. (Figure 2-5b, c, and d).
3. Two rectangular cuts were made on the top layer outlining the reservoir contours of the bottom layer. (Figure 2-5e).
4. Two reservoirs were made by cutting a glass pipette into two two-centimeter tubes. They were integrated on the pump using a 5-minute epoxy glue. (Figure 2-5f).

One of the most important advantages of PDMS is that it is easy to fabricate and allows a simple sealing with the planar substrates. However, PDMS has three significant problems in practical use.

- Dissolution or swelling by organic solvents.
- Absorption of chemical materials.
- Adhesion between PDMS and metal layer is not intact/perfect

To overcome these problems, we have coated PDMS with perfluoro amorphous polymer on the PDMS micro structures, which minimizes the problems of PDMS [40].

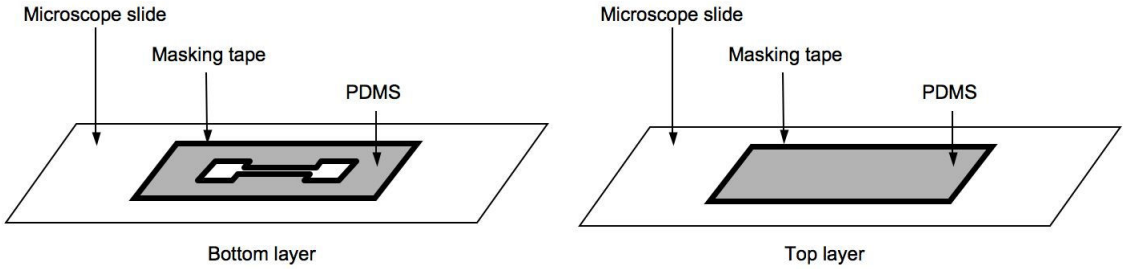

a. PDMS on two substrates to create a bottom layer and a top layer of the microchannel pump

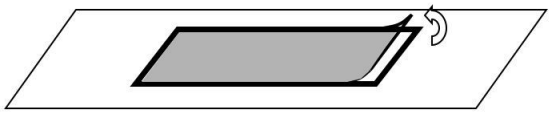

b. Top layer PDMS was peeled from the substrate after thermally cured

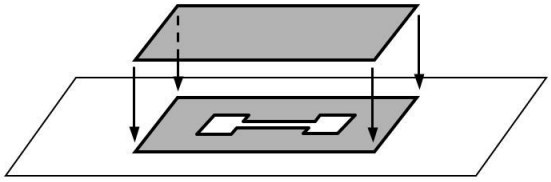

c. Top layer PDMS was placed on top of the patterned bottom layer

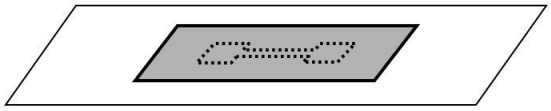

d. Top view of the sealed microchannel pump

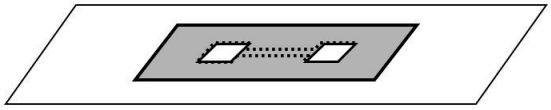

e. Two rectangular cuts were made for reservoirs

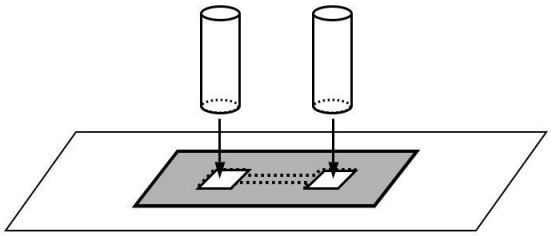

f. Integrating the reservoirs onto the pump

Fig. 2-5. Steps of fabricating microfluidic chamber

Perfluoro amorphous polymer (CYTOP, CTX-809A, Asahi Glass Company, Japan) is coated by spin coating on the PDMS structure. Since natural PDMS surface repels CYTOP, so we used O2 plasma pre-treatment on the surface before CYTOP coating. Our preliminary result shows that CYTOP coating was achieved without any deformation of the micro structure. This polymer based substrate with CYTOP can be used in different biological, chemical and lab-on-a-chip (LOC) applications.

The need for innovative fabrication methods to integrate higher levels of functionality into microfluidic and lab-on-a-chip devices is growing almost as rapidly as the number of potential applications for these miniature devices. The ability to make fully-integrated, multi-level fluidic systems with functional valves, pumping systems, electrical and electronic components, and other microeletromechanical system (MEMS) components is essential in order for this relatively new field to reach its full potential.

CHAPTER 3. AC ELECTROOSMOSIS

In AC Electroosmosis (ACEO), the tangential E-fields are from the same voltage source that induces ions in the double layer, therefore the changes of polarities in charges and field directions are simultaneous and cancelled out, maintaining steady ion migration. Because of fluid viscosity, the ion movement carries along its surrounding fluid and particles.

ACEO was first investigated using a pair of planar electrodes as shown in figure 3-1. In figure 3.1, a pair of electrodes is placed parallel in an electrolyte. The first half cycle of the applied signal is shown in figure 3.1(a). The double layer is produced on the electrode surface like dc electroosmosis. Therefore there is a nonzero tangential component of electric field acting on the double layer. The interaction of this tangential electric field with the surface charge creates the force according to the Coulomb's law. This force is along the electrode, which in turn puts the fluid in motion. In the half cycle of the applied AC signal, the sign of the surface potential becomes reversed, as shown in figure 3.1(b). The ions move accordingly, keeping the sign of the double layer opposite to the potential. At the same time, the electric field also reversed its direction. So in this case both surface charge polarity and the electric field direction changed. Subsequently, the force acting on the double layer is still the same direction as in the first half cycle, keeping the fluid motion unchanged.

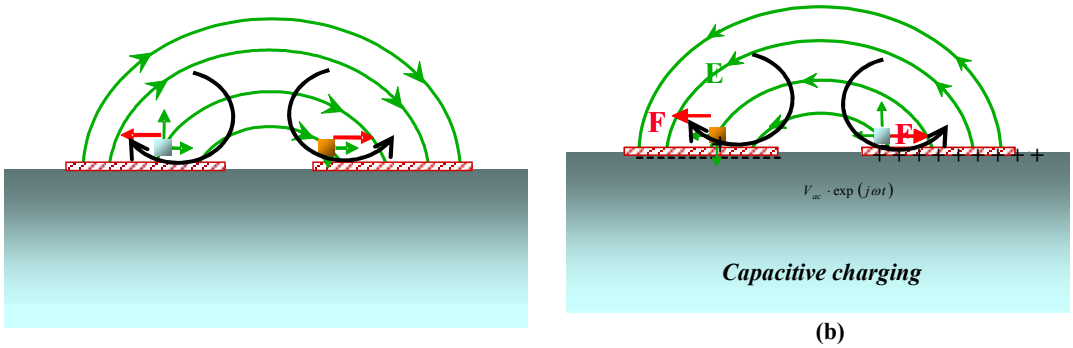

Fig. 3-1. ACEO fluid motion and induced charge at electrode surface. (a) during the half cycle when the left electrode has positive polarity; (b) during the next half cycle with opposite electrical polarity.

3.1. ELECTRIC FIELD ANALYSIS

We have used FEMLab to simulate the electric field distribution above a pair of planar electrodes (160micron width and 40 micron separation between the electrodes, with infinitesimal thickness). As shown in Fig. 3-2a, tangential electric fields change directions over one electrode, which indicates that two counter-rotating vortices exist on one electrode, as schematically drawn in Fig. 3-2b, countering to one vortex reported in the litereature.

The fluid velocity on the electrode surface is given [5] as

$$u = -(\varepsilon/\eta)(\xi - \varphi_b)E_t \qquad \text{(Eq. 3-1)}$$

where ε is the permittivity, η is the viscosity of bulk solution, $(\xi - \varphi_b)$ is the difference of potential between the double layer and the bulk solution, E_t is the tangential component of electrical field. According to Equation 3-1, the velocity on the surface of double layer is proportional to the tangential field and potential difference between the double layer and fluid, which corresponds to the normal component of electrical field. Therefore, normalized boundary conditions on both electrodes are given as, $u = -E_x E_y$.

To model the fluid motions, the 2D Incompressible Navier-Stokes module is used in FEMLAB. In this case, the hydrodynamic property in the chamber is given as density = 1000 $kg.m^{-1}$ and viscosity = 10^{-3} $kg.m^{-1}.sec$. The fluid velocity distribution is then obtained by solving Navier-Stokes equation with calculated field profile.

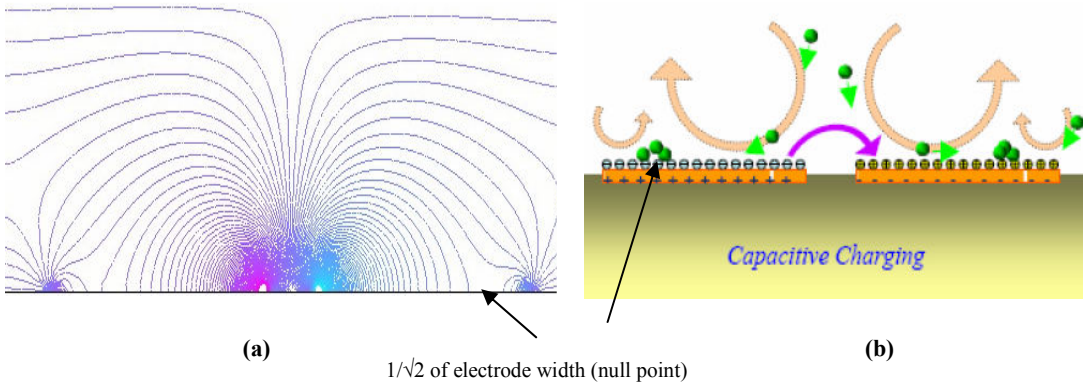

Fig. 3-2. (a) FEMLAB simulation for the Electric field distribution above a pair of planar electrodes with voltage of +1V & -1V in two electrodes (160/40micron). (b) Four counter-rotating vortices are formed above the electrodes due to changes in tangential electric fields, which facilitates particles aggregation on electrodes.

3.2. IMPEDANCE ANALYSIS FOR OPTIMIZATION

The charging and ion migration process at electrodes can be represented by an equivalent circuit element. To analyze the effect of ACEO, it is necessary to develop an RC equivalent circuit for the pair of electrodes. Fig. 3-3(a) is the equivalent circuit for the planar electrode in an aqueous environment. There are two paths that the planar interdigitated electrodes are connected as shown in the figure. One path goes through C_{cell}, which stands for the direct dielectric coupling between electrodes and it jumps the dielectric coupling through the fluid, and the environment. The other path goes through the fluid, which can be treated as resistance since it obeys Ohm's law. It is in series with capacitance for double layer charging at the interface of electrolyte and electrode on both ends. Fig. 3-3(b) is the simplified RC equivalent circuit model. At low frequency, the reactance from double layer capacitance is high. Thereby a large portion of voltage drop happens within the double layer, suitable for the ACEO phenomenon to take place. At high frequency, time is limited for double layers to form, consequently inducing a great amount of surface charge in the double layer.

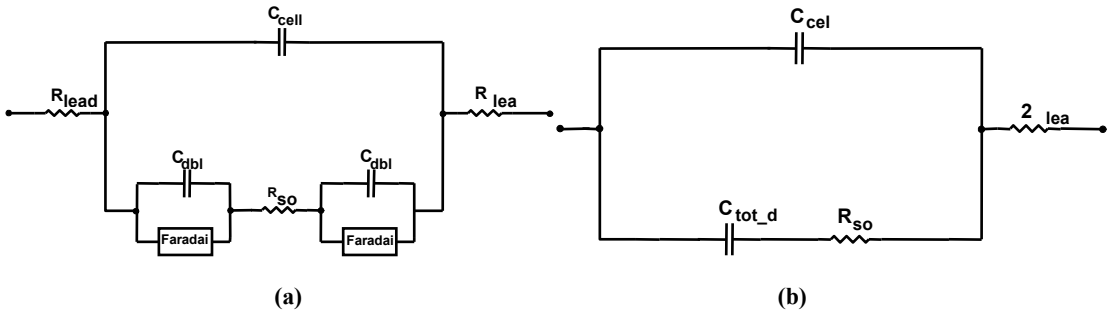

Fig. 3-3. Equivalent impedance for interdigitated pattern; (a) RC equivalent circuit for planar electrode configuration; (b) Simplified RC equivalent circuit for the modeling.

So, for the high frequency case the reactance gets smaller and more voltage drop across the resistive bulk fluid. As there is little voltage drop, hence little surface charge on the electrode, so ACEO becomes negligible at high frequency. By using the equivalent circuit model we can theoretically analyze the frequency range for the ACEO mechanism.

The values of the above mentioned components in the equivalent circuit can be extracted by impedance measurements. 5 mVrms excitation level was used for impedance measurement. For 5 mV excitation level in can be very well assumed. In this condition faradaic charging will not take place, so we neglected the faradaic charging (Fig. 3-3b) for this analysis. The simplified equivalent circuit is shown in Fig 3-3(b). Following is the modeled impedance value,

$$Z_{\mathrm{mod}eled} = \left[j\frac{1}{2*pi*f*C_{cell}} \;\Big|\Big|\; \left(R_{sol} + j\frac{1}{2*pi*f*C_{tot\_dl}} \right) \right] + 2R_{lead}$$

C_{cell} and C_{dbl} can be extracted from the experimental plot. At smaller frequency the C_{dbl} is dominated and at higher frequency $C_{cell/dielectric}$ dominants. Our extracted parameters are, C_{cell} = 305 pF; C_{dbl} = 28.85 nF; R_{lead} = 18 Ω; R_{sol} = 966.234 Ω. We put all these values to our $Z_{modeled}$ and compare the plot with the experimental impedance plot from the impedance analyzer (Fig. 3-4). The two plots matched fairly, so we can conclude that our extracted modeled parameter is correct.

The impedance measurements have been done for two different situations, 1) the electrode pair in DI water, and 2) the electrode pair in the DI water seeded with particles.

We use information from impedance measurement to optimize the operating condition (signal frequency, magnitude etc.) of ACEO.

Fig. 3-5 shows the plot of the impedance variation after adding the particles and it clearly shows the impedance differences at the lower frequencies. At first we measured the impedance of the two electrodes in the tap water (dashed line on figure 3-5). Then we measured the impedance of the electrodes for the particles (10^6 particles/ml) suspended in DI water.

Impedance plot for the two different excitation levels are also compared in figure 3-6. As seen from the figure, for high excitation voltage the impedance goes down. This is because the charge, Q is constant in the double layer, and the double layer capacitance is inversely proportional to the applied oscillator voltage (Q=CV). That is the reason the impedance plot for the two different excitation levels are different.

Nyquist plot shows the frequency response for the linear system. Figure 3-7 shows the Nyquist plot for the equivalent circuit. The low frequency area of Nyquist plot denotes the double layer capacitive effect. Point "a" denotes the solution of resistance, which we extracted from figure 3-7 is 966.234 Ω. The graphical representation (figure 3-7) using a Nyquist plot represents the two parallel path of the microfluidic system, so that we can analyze the pre-dominant of the impedance in smaller and higher frequency range. The impedance analysis is very important to distinguish the effect of different electrokinetic forces.

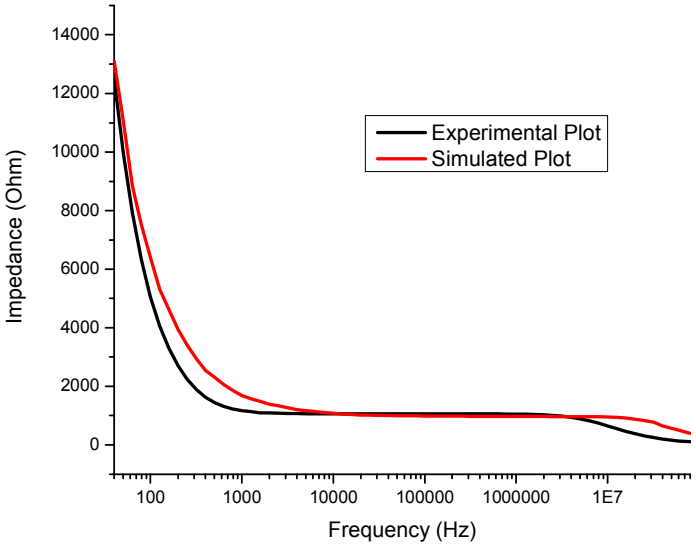

Fig. 3-4. Comparison of impedance plot between the experimental and the modeled data

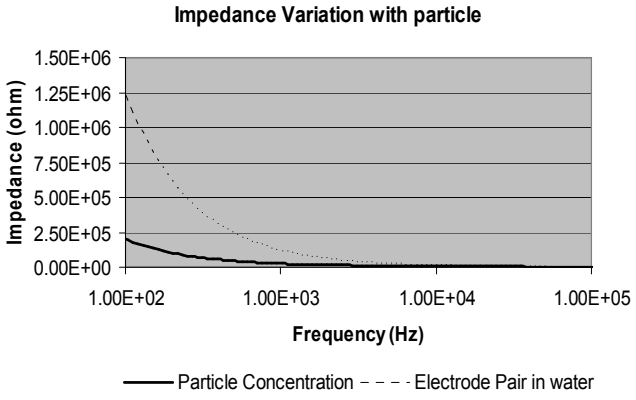

Fig. 3-5. Impedance measurement with and without the particle

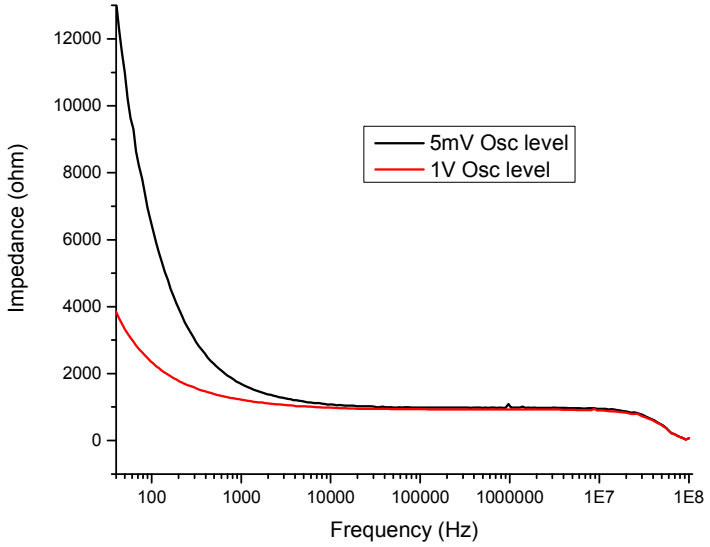

Fig. 3-6. Comparison of Plot of the impedance for two different Oscillator level for same fluid

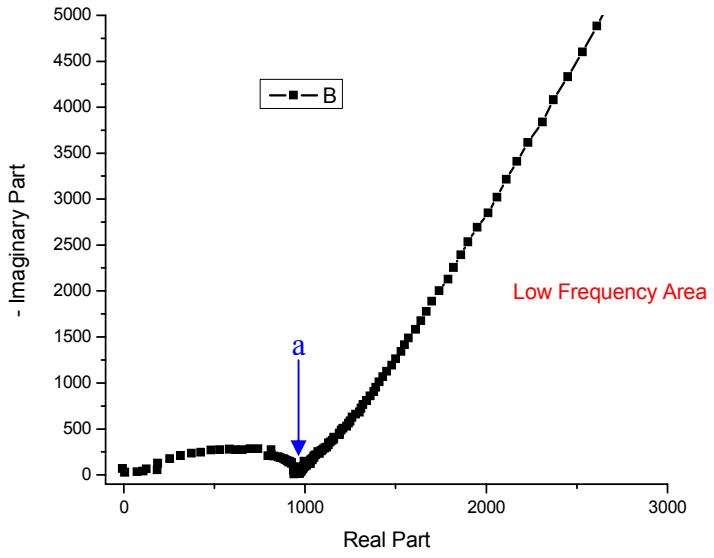

Fig. 3-7. Nyquist Plot for real vs Imaginary plot at 5mV Osc Level

From the figure 3-5 we also can see that the difference of the impedance with and without the particle is more in frequency below 1 KHz. So we adopted signal frequency range between 100 Hz to 1 kHz for particle trapping. The experiment was done at 500 mVrms oscillation level. Same characteristics were obtained at 1 Vrms. Our goal is to determine a higher velocity electrode pattern with the polystyrene particle, so both experiments and calculation were performed to determine the optimum signal magnitude for these four sizes of electrode pair (160/40, 160/20, 80/40, 80/20).

3.3. Capacitive and Faradaic Charging Effect

Biased ACEO is realized by applying biased AC signals over electrode pairs, leaving the electrolyte floating; therefore, two electrodes have different electrical potentials relative to the electrolyte. With a biased AC signal, $V_{applied}=V_0(1+\cos\omega t)$ over the electrodes, the left electrode is always positive and more prone to Faradaic charging, while the other is always negative and subject to capacitive charging.

For the biased signal one electrode has a positive offset with the potential always greater than zero, while the other one lower than zero (Fig. 3-6). When the voltage exceeds the threshold for reaction, asymmetric vortices are formed above two electrodes as faradaic reactions take place at the positively biased electrodes. Faradaic reaction generates co-ions following Faraday's law. For the other electrode with a negative offset, counter ions are attracted to the electrode. Therefore, for two electrodes, same polarity of ions is induced. A unidirectional fluid loop is consequently formed by tangential fields, as shown in Fig. 3-6. For the negative particles in an aqueous environment, they adhere to

the stagnation line on the positively biased electrode. Henceforward, biased ACEO exhibits directional particle assembly.

Because most bioparticles are negatively charged, the DC bias can provide a synergy of AC and DC electrokinetics for more efficient particle collection. Electrophoretic/electrostatic force is exerted simultaneously with ACEO to move bioparticles towards positively-biased electrodes, as shown in Fig. 3-6. It is also showed in the next section with the experimental result that the DC biased electrode configuration will introduce a large number of surface charge on the electrode, which will introduce the higher fluid velocity.

Figure 3-6 already explained the electric field direction and net fluid flow for the asymmetric biased electrode pattern. Also in next section we have experimentally proved unidirectional particle flow. Breaking the charging symmetry on electrodes are main concept of producing uni-directional flow. With the biased AC signal, one electrode is at a higher voltage and hence undergoes Faradaic charging with cations, and the other electrode is at a lower voltage and hence is polarized by capacitive charging with the cations as well. This combination of the two polarization on the two electrodes of an electrode pair produces a uni-directional flow on each of the electrode pairs on electrode array. Which eventually produce a continuation of fluid flow and show the pumping action. The pumping action is described thoroughly in Chapter 5, where we also have shown the possibility of increased velocity by decreasing the channel height of micro-chamber.

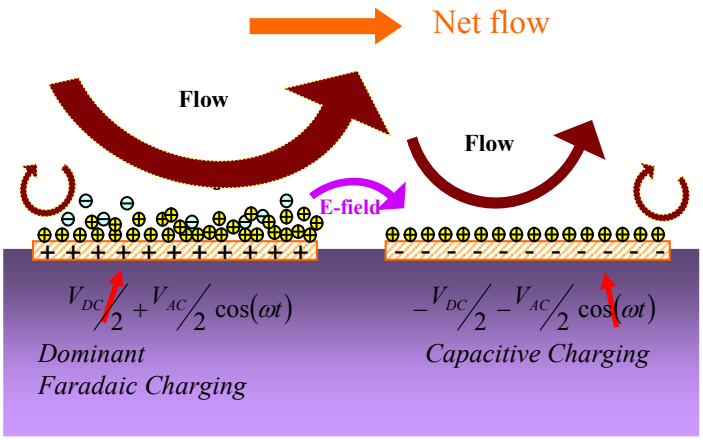

Fig. 3-8. Asymmetric polarization with appropriate magnitude can produce uni-directional net flow.

3.4. EXPERIMENTAL RESULT

ACEO flow is examined using microfabricated arrays of electrode pairs on silicon substrate. Au/Cr (90nm/10nm thickness) electrodes were fabricated by lift-off procedure in IC processing. Cr is the adhesion layer between the substrate and Au, and Au is in contact with electrolytes. The electrodes were 20 mm long, 0.1 μm think, 80 μm wide with a 20 μm separation (denoted as 80/20). Microfluidic chambers were formed by sealing silicone microchambers (PC8R-0.5, Grace Bio-Labs, Inc.) over the wafer, which have a height of 500 μm. Polystyrene spheres (1 μm diameter; Fluka Chemica) seeded in DI water was used to track fluid motion.

Fig. 3-7(a) shows the initial distribution of particles when no signals are applied over the electrodes. Fig. 3-7(b) shows that particles accumulated from both sides into lines at approximately $1/\sqrt{2}$ of electrode width [12]. This corroborates the theoretic prediction, since fluid velocity reduces at the null points of electric fields, and particles become trapped to the electrodes due to surface forces of between particles and electrodes.

ACEO can transport the particles from a large region in the bulk fluid to the electrode surface. The flow velocity is important for optimizing the micropump and particle transportation. In contrast to electrophoretic and dielectrophoretic (DEP) velocity, which are typically limited to less than 20 microns per second [9], the ACEO velocity exceed 100 micron/sec.

Fig. 3-8 gives the comparative analysis of the microfluidic velocity generated

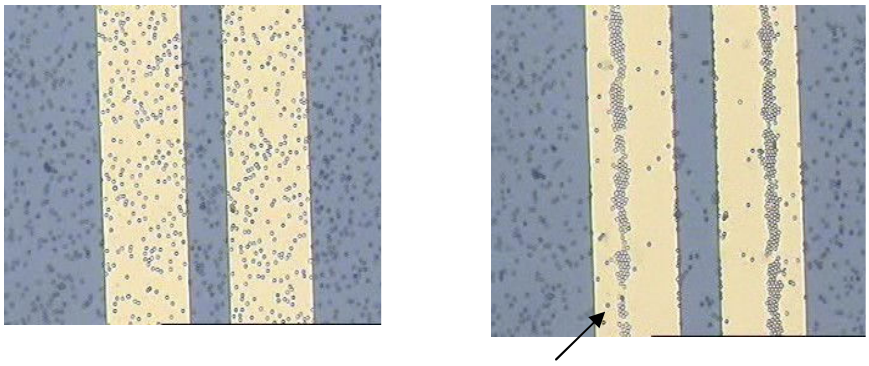

Fig. 3-9. (a) Particle without the supply voltage (b) Experimental picture of the particles accumulating at the 1/√2 electrode width;

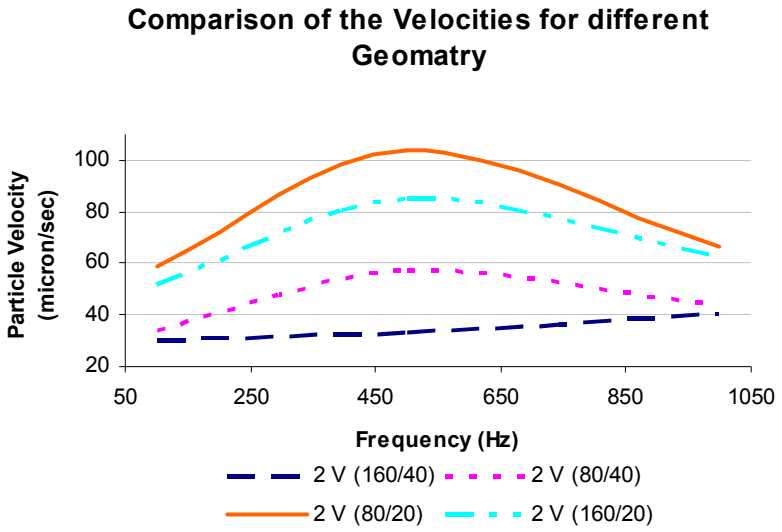

Fig. 3-10. Microfluidic Experiment result & comparison of four types of electrode geometry

using four types of Au electrodes. The 80/20 configuration gives the highest velocity, which is suitable for the pumping application.

Here we have also compared the particle velocity for symmetrical biased and asymmetrical biased signal pattern. The experimental fluid velocity generated by A-P ACEO is summarized in Fig. 3-11. When the voltage exceeds the threshold for reaction, asymmetric vortices are formed above two electrodes as Faradaic reactions take place at the positively biased right electrode (Fig 3-11).

From our earlier experiments we learned that 80/20 configuration provides higher particle velocity, we have used this electrode configuration in our A-P ACEO experiments. Our experimental result (Fig. 3-12) suggests that the velocity from asymmetric biased electrodes is much higher than that from symmetric biased electrodes.

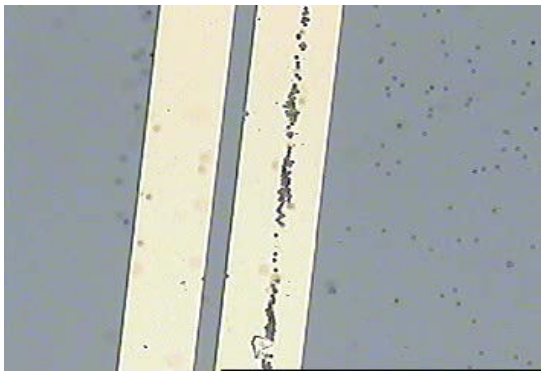

Fig. 3-11. Biased ACEO fluid flow; Experimental result shows the particles deposit only on positive electrode

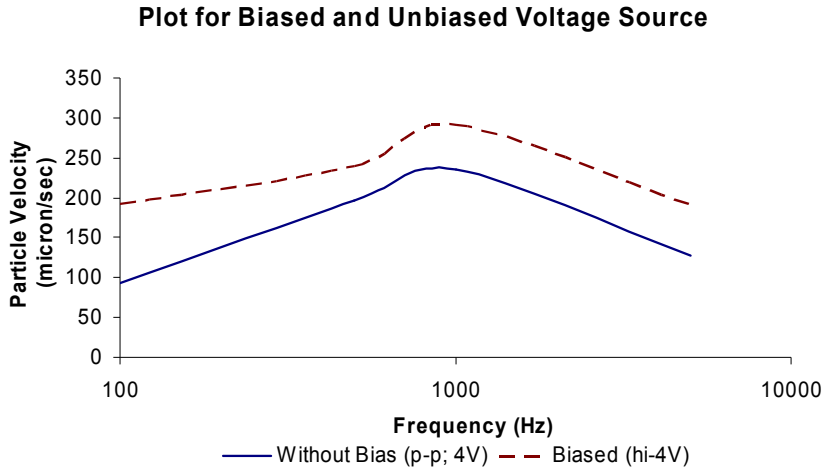

Fig. 3-12. Flow Velocity Comparison for the ACEO with DC bias of 1.5V and without bias

For the biased ACEO experiments, applied voltage exceeds the threshold for reactions at V_0=1.5V (i.e. high level & low level of biased voltage is 3V & 0V respectively). At the same voltage, the maximum flow velocity shifts to higher frequency compared with symmetric AC signals (Fig. 3-10). This is because Faradaic polarization becomes suppressed at high frequency. Beyond 500Hz, microflows from capacitive charging are much stronger than those from Faradaic charging, so that the stagnation point on the left electrode disappears. At 100Hz, streamlines from capacitive charging and Faradaic charging become connected, forming a large vortex over the electrode pair and the particles aligned on the right electrode (figure 3-11).

3.5. Experimental and Analytical Validation of Electroosmotic Flow

Particle displacement is also affected by the gravity, dielectrophoresis (DEP) and Brownian motion, so we have used the following equations to calculate the distance that a particle will travel under those forces in a single second, for our simplified microelectrode structure.

$$Gravity = 0.2\frac{a^2\rho_m g}{\eta}t \tag{3-2}$$

$$Dielectrophoresis(DEP) = 0.03\frac{a^2\varepsilon}{\eta}\frac{\left(cV^2\right)}{r^3}t \tag{3-3}$$

$$BrownianDisplacement = \sqrt{\frac{k_B T t}{3\pi a\eta}} \tag{3-4}$$

DEP displacement is inversely proportional to the r^3 (where, r = spacing between the electrodes, characteristic length). For this reason 80/20 configuration produces 8 times stronger DEP than does 80/40 configuration. We have noticed that for higher

electric field intensity at the edge (from simulation), the particles had the highest velocity at the inner edge of the interdigitated electrodes.

The particle size, a, is important factor for these forces. Gravity is proportional to the a^2 but Brownian displacement is inversely proportional to $\sqrt{a}$. To decrease the gravitational displacement we certainly need to move to the smaller particles, though the Brownian motion increases.

As we have used the 3 μm particle, the displacement due to Brownian motion (Eqn. 3-4) is negligible. But the gravitational force is more dominant (Eqn. 3-2) compare with the Brownian motion. The value of DEP, gravity and Brownian displacement in a sec is 0.926, 0.202 and 0.0128 micron, for 80/20 electrode configuration, which is negligible compare to the experimental ACEO displacement per second.

CHAPTER 4. INTEGRATION WITH MICROCANTILEVER

We have investigated another microstructural design for ACEO devices, which is similar to a pair of parallel plates (Fig. 4-1). In this configuration, electrodes are facing each other, similar to a pair of parallel plates. The two face-to-face electrodes are asymmetric in design, so they produce non-uniform electric field. For mechanism identical to that of planar electrodes, surface EO flows are generated from the electrode edges inwards, and slow down to stagnation at the center, where particles are expected to trap.

4.1. ELECTRIC FIELD ANALYSIS OF PARALLEL PLATE PARTICLE TRAP

Most ACEO devices reported so far adopt a side-by-side (interdigitated) configuration. To integrate such design on microcantilevers would call for sophisticated microfabrication. We use a face-to-face configuration, very much like a pair of parallel plates, with one plate having smaller electrode area than the other, as shown in Fig. 4-1. As the top and bottom electrodes are asymmetric, the tangential electric fields are generated which induces electro-osmotic fluid motion. For the first half cycle as in Fig. 4-1a, the bottom electrode is at positive potential, and negative ions are induced at the interface of the electrode and fluid. These negative ions interact with the electric field and produce two counter-rotating vortices from electrode edges inward on the electrode surface, creating null point at the center of the electrode.

For the next half cycle as in Fig. 4-1b, applied potentials switches polarity and the bottom electrode is at negative potential. Here the induced positive ions will interact with the electric field and again produces two counter-rotating vortices from electrode edges inward, and fluid motions are sustained thus the particles are trapped at the center of the electrode. As the bottom plate is smaller than the top plate, the electric field is almost always normal to the top electrode, hence tangential force can be neglected.

The tangential electric field for the asymmetric electrode pattern induces electro-osmotic fluid motion in the bottom plate. It is the microfluidic flow that conveys particles from the bulk of the fluid onto the fluid surface. The stagnation point created at the center of the bottom plate. The particles are trapped at the stagnation point of the fluid.

The advantage of the parallel plate configuration is it can be interfaced with the sensors. It can also accommodate large volume of liquid compare to the interdigitated electrode pattern. By having different electrode configuration, different types of particle patterning can also be possible. With different types of particle patterning, the device can be used with different applications. This application specific patterning makes the use of parallel plate configuration versatile. Another advantage of parallel plate configuration is, it can be interfaced with other sensor devices. In our research we integrate microcantilever with our AC-EO parallel plate configuration. It opens the door to interface with other sensor, and make the whole system ultra-sensitive for bio / chemical analysis.

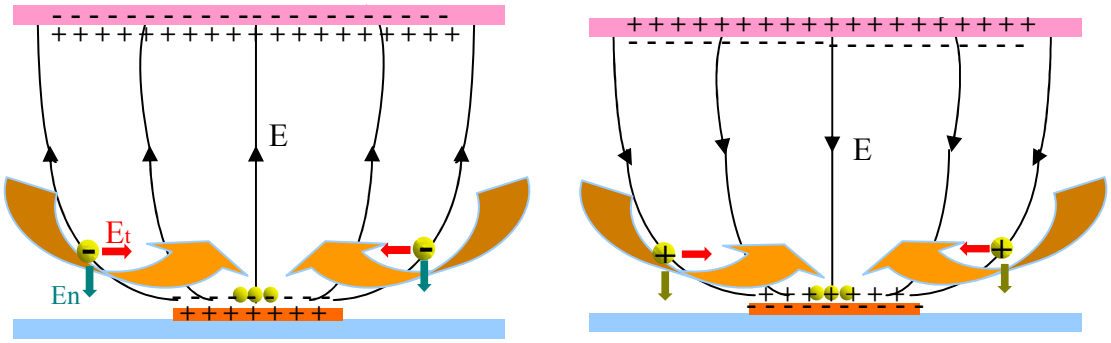

Fig. 4-1. Concept of Parallel plate particle trapping for an AC cycle; (a) during the half cycle when the bottom electrode has positive polarity and ITO coated top electrode is negative; (b) next half cycle with opposite polarity. Flow motion and induced charges is also shown

4.2. EXPERIMENTAL SETUP AND RESULTS

The initial particle trapping experiments were performed using two plate electrodes; the bottom plate is patterned gold (Au) electrode and the top plate is an indium-tin oxide (ITO) coated glass slide (Fig 4-2). The patterned electrodes are fabricated by electron beam evaporation and lift-off into the form of "#." The two electrodes were separated by a 500µm silicone spacer. Particles with sizes from 200 nm to 3 µm were suspended in de-ionized (DI) water. An Agilent 33220A signal generator was used to apply electrical potential to electrodes. A frequency range from 100 Hz to 1 kHz was determined to be optimal for observing particle motion in the DI water suspension [13]. The particle movement was observed using Nikon LV100 microscope through the glass top plate, which also conduct electricity through ITO.

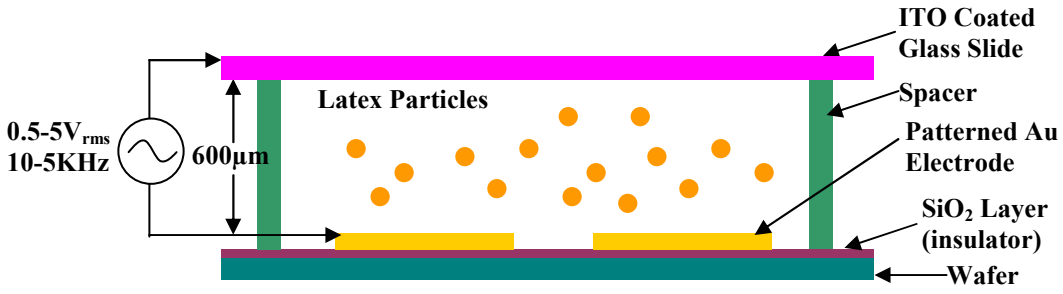

Fig. 4-2. Schematic of the experimental setup of Parallel Plate configuration particle trap

Fig. 4-3 shows that particles form lines along the center of conductive electrode strips. In Fig. 4-3(a) and Fig. 4-3(b), the brighter area denotes the conductive layer. Various trapping patterns can be realized by patterning the electrode differently. With 3μm particles we can see some DEP effect at the edge of the electrodes [18]. To minimize the DEP effect we have used 200nm particles for trapping, thus gravitational effects are also minimized. The conductivity of the particle solution is 7.8μS/cm, so we can also neglect the electrothermal effect [19].

4.3. Optimization of Parallel Plate Particle Trap

By changing the separation between the two plates, the electric field strength is varied, therefore changing the flow velocity. We have used the double sided tape between the two parallel electrodes, so that we can control the separation between them. A separation of 380 μm is used in experiments.

The particle trapping process is a function of the frequency and magnitude of the applied signal. Intuitively, the flow velocity increased with the applied voltage due to higher electric field strength. Fig. 4-4 also shows the frequency dependency of the fluid velocity for parallel plate configuration. The experimental results show the highest velocity at the edge of the bottom electrode.

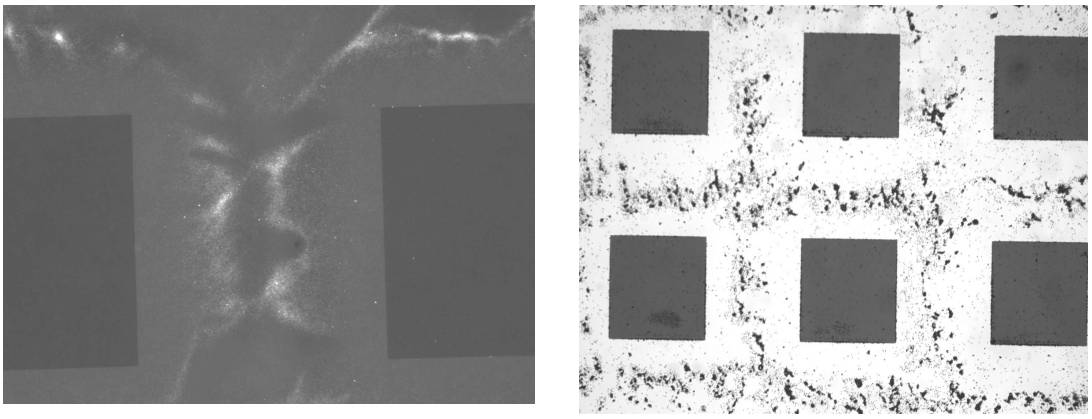

(a) (b)

Fig. 4-3. Experimental result of particle trap; (a) Parallel plate 200nm fluorescent particles start trapping at the center of the conductive metal layer; after 2mins of applied signal; (b) Experiment result using 3 μm particles. Bright areas are electrodes and dark areas are substrate. Particles are trapped on the centre of Electrodes.

As the sign of the AC electric field changes the ions of the double layer also changes, i.e. there is a continuous process of in and out of the ions. For higher frequencies, the ions in the double layer capacitor have less time to redistribute [20] as the AC electric field changes polarity. That is why flow velocity decreases at high frequency. For the very low frequency case, there is plenty of time for the double layer capacitor to charge up to practically the same voltage as the input; eventually creating zero electric field inside the chamber and there is no ACEO flow. As shown in Fig. 4-4, electric fields with frequencies around 500Hz create the higher velocity. Needless to say, the velocity of the particle is higher (higher electric field density) at the edge and goes down as the particles approach the null point.

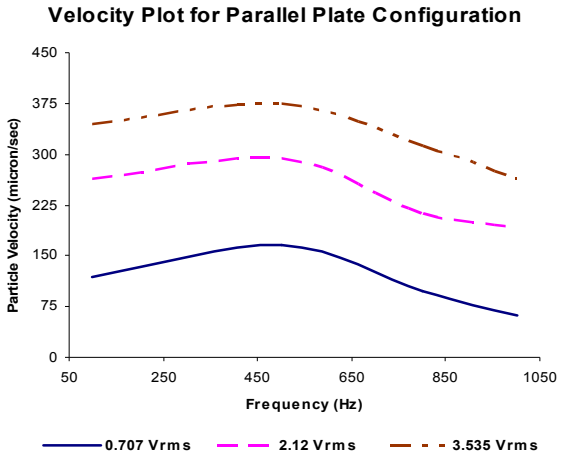

Fig. 4-4. Experimental particle velocities with respect to frequency at the edge of conductive layer for three different voltages,

4.4. MICROCANTILEVER PARTICLE TRAPPING

This section explains the novel particle trapping method using microcantilever. Here we have presented the first integration of the microcantilever with the ACEO particle trapping mechanism.

4.4.1. Microcantilever as Mass Sensor

Recently microcantilever sensor technology has boomed and become a promising sensor technology. Microcantilever sensors have several advantages over many other sensor technologies, including faster response time, lower cost of fabrication, the ability to explore microenvironments, and improved portability.

Cantilever resonance responses, such as frequency, deflection, Q-factor, and amplitude, undergo changes due to adsorption or changes in environment. Resonance frequency of a microcantilever can be used to detect particles. When the target is loaded on the microcantilever, the resonance frequency of microcantilever is going to change. That means for the mass loading on the cantilever the resonance frequency is supposed to go down.

As shown in Fig. 4-5, the microcantilever resonance frequency is f_1 without any additional mass. The frequency response of microcantilever is also shown. When we add a small mass Δm the resonance frequency of the microcantilever is changed to f_2. As we can see from the resonance frequency equation, in this case the resonance frequency will go down for additional mass loading. The frequency response also reflects the resonance frequency change for the mass loading.

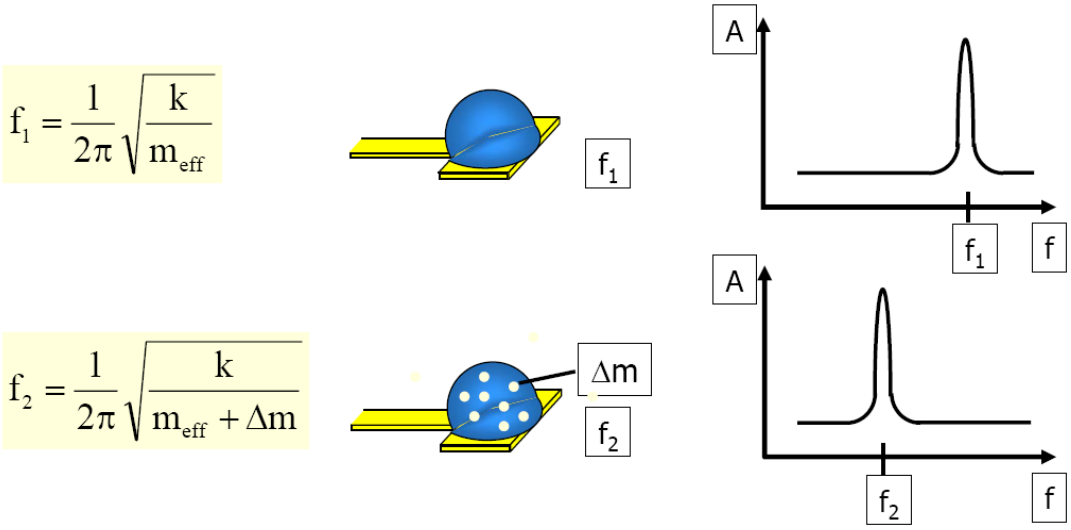

Fig. 4-5. Microcantilever responses on resonance frequency for a small mass loading

4.4.2. Integrating Microcantilever with ACEO

The parallel plate design has been used to attract particles onto cantilevers for high sensitivity detection [14]. Because particle trapping/concentrating effect is more obvious with the smaller electrode, in our design the metal-coated cantilevers are facing one large electrode (covering a whole fluid chamber), so that particles will aggregate on the cantilevers.

The tangential electric field of parallel plate configuration is generated for the asymmetric electrode pattern, which induces electro-osmosis fluid motion. FEMLab simulation in Fig. 4-6 shows that induced osmotic flows direct from outer edge of the cantilever to the center. Therefore, two main loops are formed with particles trapped onto the center of cantilever.

In our design of microcantilever trap, the metal-coated cantilevers substitute the patterned bottom electrode, so that particles will aggregate on the cantilevers [15]. Fig. 4-7 shows the experimental setup of cantilever particle trap. As shown in Fig. 4-7, photoresists (dielectrics) are coated on the conductive areas other than the cantilevers to suppress unwanted local EO flows. The ITO glass slide works as the top electrode, which is covering the whole fluid chamber. We have used Au-coated AFM probes as the MC, which has the dimension of 125μm X 30μm X 4μm. Tipped MC side was not used to avoid sharp electric fields.

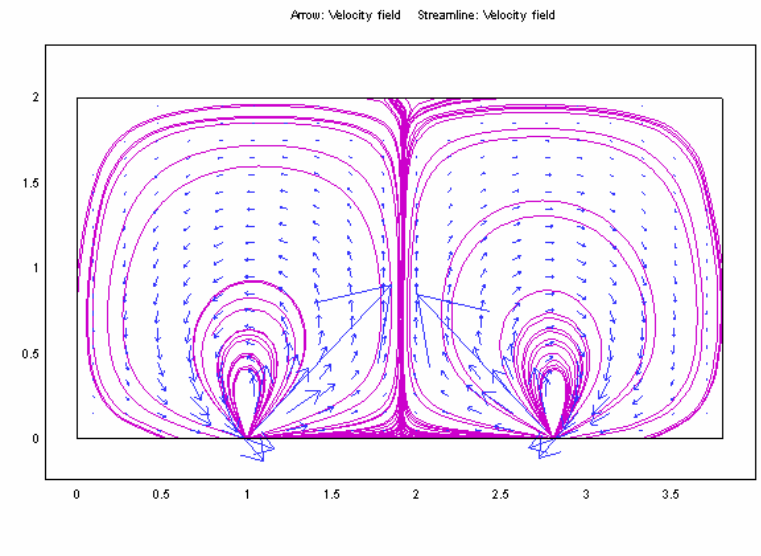

Fig. 4-6. Calculated velocity plot indicates osmotic flow within the chamber, causing the stagnant area and particle trapping

Fig. 4-8 shows the experimental results of trapping 200nm fluorescent particles on MC. After applying the AC signal (100Hz, 400mVp-p), suspended particles accumulate at the center of the cantilever from all directions. As time passes, more fluorescent particles from the surrounding area accumulated and formed bright object pattern.

After the particle trapping on the surface, the MC was dried with AC signals applied, so that particles will not get dispersed by diffusion, surface tension, etc. As shown in Fig. 4-9, particles are still concentrated at the center after fluid dryout. Then the particle trapping effect was verified with AFM resonance measurement.

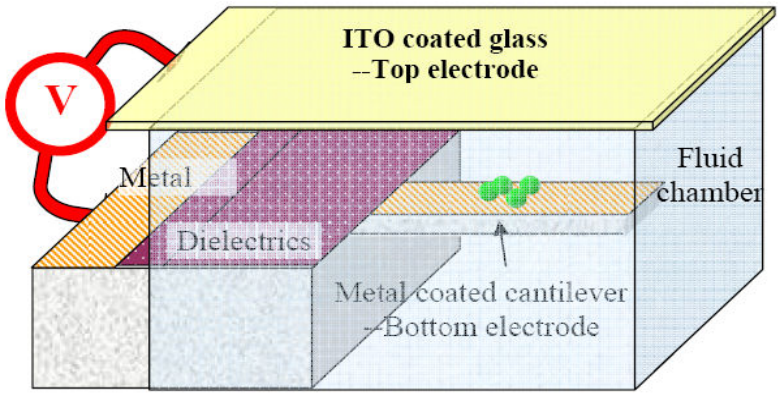

Fig. 4-7. Experimental Setup of Cantilever particle trap

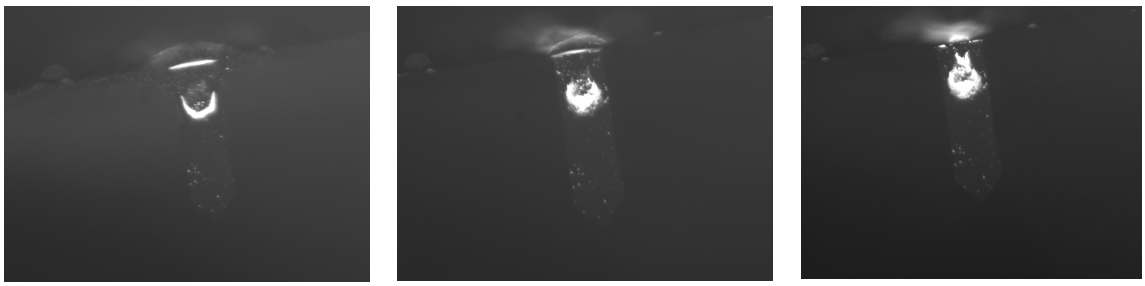

(a) **(b)** **(c)**

Fig. 4-8. Image sequence of 200 nm fluorescent particles trapped on the micro-cantilever; (a) t = 10 min, (b) t = 20 min, (c) t = 30 min.

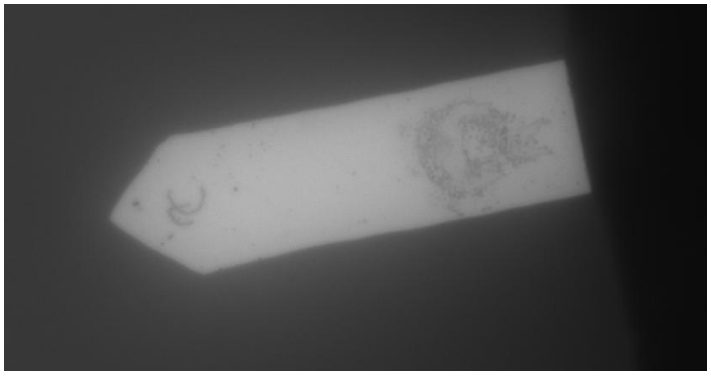

Fig. 4-9. Micrograph of nano-particles trapped on microcantilever after the solution evaporated away.

4.5. PARTICLE TRAPPING VALIDATION

To verify the concentrated particle trapping on MC, we also measure the resonance frequency of MC before and after trapping experiments. MC resonance frequency is inversely proportional to the differential mass of cantilever [21]. The sensitivity of a cantilever to mass loading is mainly determined by the excited cantilever resonance frequency.

$$\Delta m = \frac{K}{4\pi^2}\left(\frac{1}{f'^2} - \frac{1}{f^2}\right) \tag{4.1}$$

Where, Δm is the mass change;

K=sensor spring constant;

f = resonance frequency before mass adsorption;

And f' is the resonance frequency during mass adsorption.

Changes in the mass and surface properties of the microcantilever through binding or hybridization of analytes to receptor molecules will directly influence its surface stress. This causes the microcantilever to deflect and the deflection is proportional to the analyte concentration and inversely proportional to mass loading. The more the particle concentration on ACEO-cantilever, the more is the bending. So the more mass on the cantilever means the lower resonance frequency. From our experimental result (Fig. 4-10) we have got the resonance frequency of the MC goes down to 276.07 KHz after particle trapped on the MC for ACEO, which translates to a change of mass. For a change in mass we get,

$$\frac{f_1}{f_2} = \frac{\sqrt{m_{eff} + \Delta m}}{\sqrt{m_{eff}}} \tag{4.2}$$

Microcantilever dimension is 125μm x 30μm x 4μm. The volume of the MC is $1.5e^{-14}$ m^3. Microcantilever is Si based, and the density of Si is 2330 kg/m^3. So the mass of microcantilever is $3.495e^{-8}$ gm. By putting the frequency and mass values in equation (4.2), we have got an increase of 2.52% increase of mass for the frequency change from 279.52 KHz to 276.07 KHz.

The change in resonant frequency as a function of the particle mass binding on the cantilever beam surface forms the basis of the particle detection scheme.

4.5.1. Analysis of Particle Trapping Using SEM

Our research also shows that applying the electric field creates a certain crystal shape of the concentrated particles. Without applying the electric field, the particles are accumulating in layers, and formed no crystal shape (Fig. 4-11a). But when the electric field was applied for ACEO, the particles formed the close-packed layer of colloidal particles, and take the shape of crystalline structure, as shown in Fig. 4-11(b). Compare with the Fig. 4-11(a), the crystalline structure (Fig. 4-11b) increases the number of particles in the bottom layer [22].

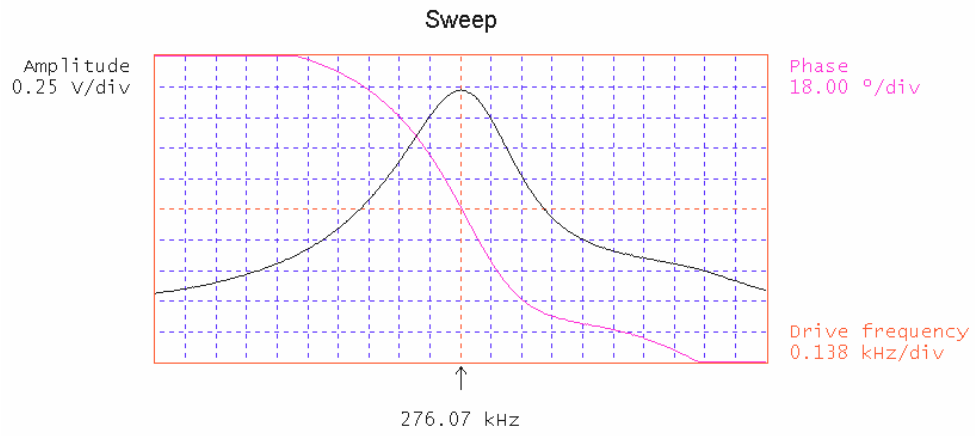

(a)

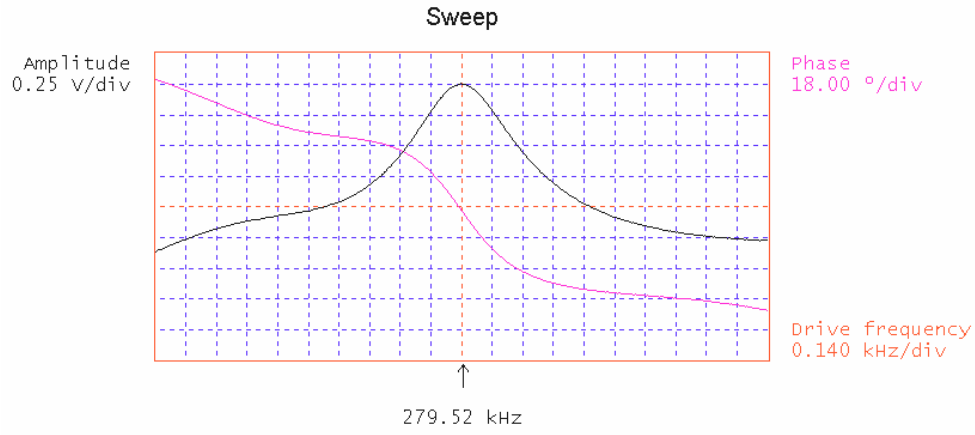

(b)

Fig. 4-10. Resonance frequencies of the MCs (measured with multimode AFM.) (a) After the particle trapping by ACEO, 276.07 kHz, (b) Control experiment with no electric signal applied, 279.52 kHz.

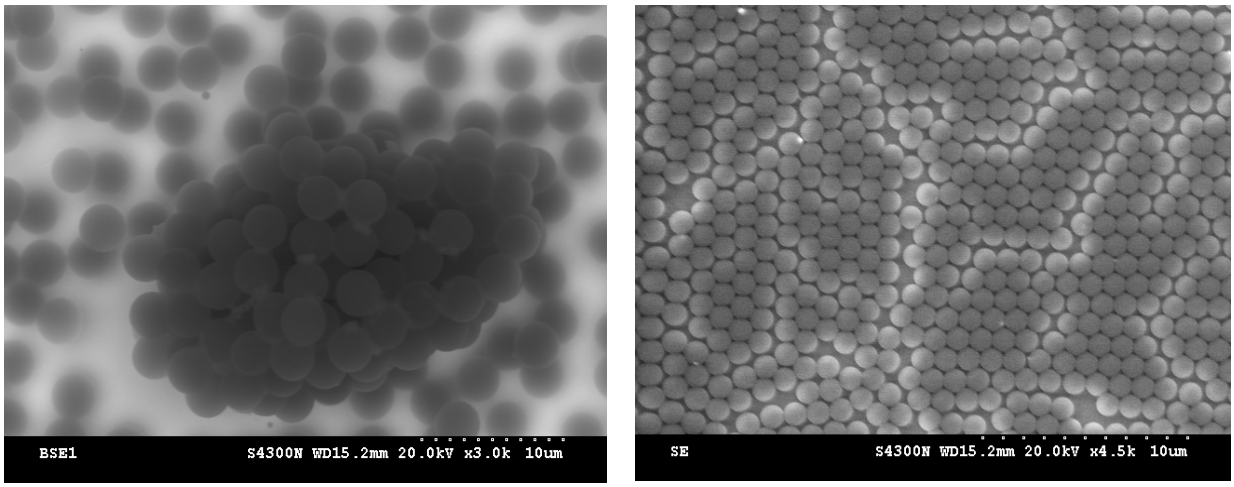

(a) (b)

Fig. 4-11. SEM image of the particles; (a) Particles dried on the surface, no electric field is applied (b) For ACEO particle trapping, particles take the Crystal Shape.

CHAPTER 5. AC ELECTROKINETIC MICROPUMPS

5.1. INTRODUCTION

Micropump is critical to transport small amounts of fluid for many microfluidic applications, ranging from drug delivery, bio-fluid analysis, to microelectronics cooling. With the development of MEMS technology, micropumps have been designed and fabricated to integrate with lab-on-a-chip.

Due to the large surface to volume ratio in microchannels, surface tension and viscous forces play an important role in the flow characteristics. So for micropumping action we need to choose the electroosmosis technique which benefits from the higher surface to volume ratio. For this reason electroosmotic action is suitable for miropumping action.

Electroosmotic (EO) pumping is the motion of bulk liquid caused by the application of an electric field to a channel. Electroosmotic (EO) pumps (a.k.a. electrokinetic pumps) have no moving parts and are capable of generating high flow rate per device volume. People use electroosmotic pumping to achieve both significant flow rates and pressures, and a fairly wide range of working electrolytes may be used (including deionized water, buffered aqueous electrolytes). These devices have significant pressure capacity in a compact structure. We have achieved flow rates in

excess of 400 micron/second. EO pumps offer some advantages over other miniature pumps for microchannel cooling applications and integrated bio-analytical systems.

High-pressure capacity, millimeter-scale, porous-media based EO pumps have been demonstrated [71, 72], and most of the micropumps which are presented in the literature are DC-EO micropumps. However, DC EO micropump suffers from high voltage operation (several kVs) and consequently excessive electrochemical reactions and electrolysis at the electrodes. This high voltage operation also creates the pH gradients and bubble which is not favorable for micropumping [56-61]. Again, many of the current fabrication techniques of porous-media EO pumps are not compatible with standard microfabrication processes and this poses a significant obstacle to the chip-level integration of EO pumps into microsystems. Our developed micropump is operated with smaller AC voltage and microfabrication compatible.

Reliability, compatibility, and cost are also criterions for selecting or designing micropumps. Micropumps must perform proposed functions without being damaged (re-usable), and at the same time must not bring changes in the medium. Compatibility with microsystems requires precisely pumping the desired range of fluid volumes and proper overall size of the micropump. Micropump can be used to manipulate the fluid volumes ranging from a few picoleters to hundreds of microliters for different biomedical applications, such as single molecule detection, species separation, antigen-antibody binding. The pump size is important for integrating the compact microsystem. The simplicity in design and fabrication of micropumps is also desirable. By using our

fabricated micro-electrode array the problems of the electrokinetic micropumps can be solved.

Ajdari *et al* have already developed an integrated electrokinetic miropump, driven by a low AC voltage [45]. They have used 120 repeated asymmetric pair of electrodes. In this research we have used the biased AC electroosmosis to produce the unidirectional fluid flow in the symmetrical array of the electrode pattern. Next sections have described in details of AC electroosmosis micrpump and demonstrated the simulation and experimental result of pumping action.

5.2. Brief Review of Micropumps

A variety of micropumps has been made to transport small amount of fluids. An excellent review is given by Laser and Santiago [46]. Micropump classification is illustrated in figure 5-1, which is on the basis of Krutzch and Cooper [47]. In general, the micropumps can be organized into two categories, with or without moving parts. The ones with moving parts are often referred to as displacement micropumps. A typical displacement pump consists of a piston or moving surface, a chamber and two valves [50]. The moving parts draw and expel working fluid in suction and discharge strokes. This type of pump can provide output pressure as high as 200 kPa. However, displacement pumps usually have complicated structures and large sizes ranging from 10 mm^3 to 10000 mm^3 [46], difficult in fabrication and integration of microfluidic systems. The moving parts are not suitable for particle-laden flows in biomedical and chemical

applications. On micro-scale level, micron-sized particles such as cells and DNA maybe damaged by the moving parts and vise versa, reducing reliability of the micropumps.

Different types of micropump without moving parts have been developed as alternatives to displacement pumps. This type of micropumps are used extensively for biological and chemical analysis at microscale. In general, the micropumps provide fluid motion by applying external electric fields through viscous interactions between charges and the fluid. The charges are mobilized by different mechanisms. Magneto-hydrodynamic (MHD) and electro-hydrodynamic (EHD) micropumps are two main categories.

The key parameters that dictate the performance of EO pumps are (i) the magnitude of the applied electric field and applied voltage, (ii) the cross-sectional dimensions of the structure in which flow is generated, (iii) the surface charge density of the solid surface that is in contact with the working liquid and (iv) ion density and pH of the working fluid.

MHD micropumps can drive fluids without moving parts and hence achieve higher reliability. But the fact is that, MHD micropumps need both electric and magnetic sources for operation. Using both sources increases the complexity and makes it challenging for these pumps to be incorporated into a lab-on-a-chip system. In addition, small magnetic flux density for smaller magnetic source at the microscale limits their performance. The flow rate of MHD pump is a function of the channel dimension [48], which prevents miniaturizing the pumps.

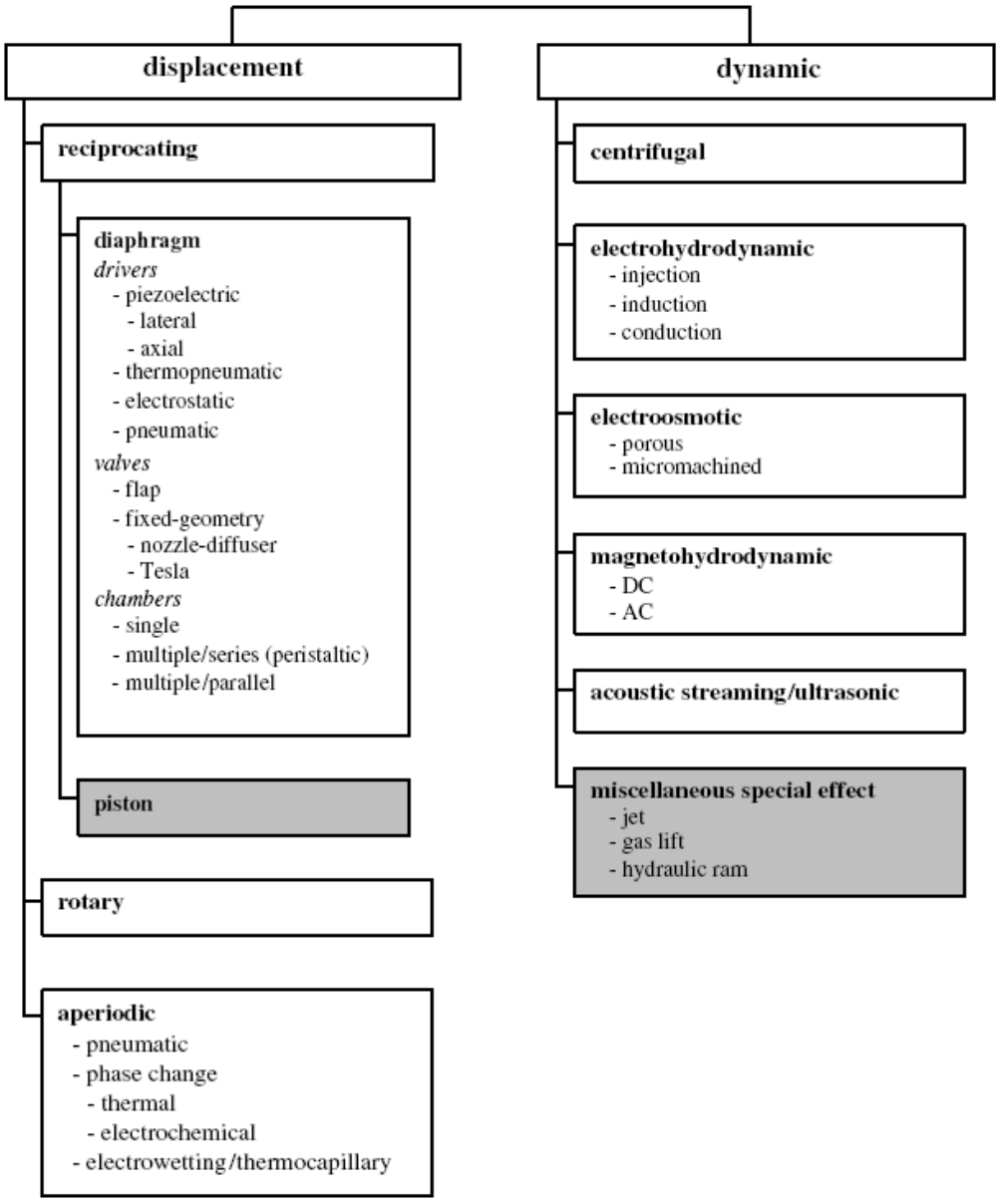

Fig. 5-1. Classification of pumps and micropumps; after Krutzch and Cooper [48].

Compared to MHD pumps, the EHD pumps need only electric fields to pump the fluids. The flow can be generated through Coulomb force, dielectric force, or both. The Coulomb force resulting from the interactions between charge and electric field is the main mechanism used in designing most EHD pumps. To produce the charge, a variety of techniques have been used. The charge can be produced by induction, conduction or injection. Induction charges occur when an electric field is applied to a fluid with an inhomogeneous conductivity. Nonuniform conductivity can be achieved by introducing the working fluid with different conductivity or imposing a nonuniform temperature field in a fluid. Electrothermal effect is associated with this category. Conduction depends on dissociation of ions when immersing a charged surface into a liquid. In the electroosmosis we introduce the charged surface inside the fluid chamber. So electroosmosis can be categorized in this group. Charges can also be directly induced through ions injection by applying high electric field.

Dielectric force can also be used to produce the fluid motion. For this case the nonunifrom permittivity is necessary to produce the dielectric force that can be created by nonunifrom heating. The detailed description of EHD pumps can also be found in the paper [48-55].

Among EHD pumps, electroosmosis (EO) pumps are widely used in broad applications, such as DNA separation, drug delivery [54-61]. ElO is already explained in the earlier chapters. As figure 3-1 shows, the applied external electric field pulls mobile ions in the double layer, resulting in a moving ion boundary, which in turn drags the bulk fluid direction of the electric field depending on the signs of surface charges.

The performance of the EHD pump is dependent on the working fluid and the surface material. The same working fluids with different surface materials may produce either positive or negative ions, which eventually determine the flow direction. Zeta potential is the key factor that depends on the fluid and the surface material. Other important factors include the applied voltage and the channel size. For a desired flow rate the applied voltage of the EO pump may vary from 100V to 10kV. Some pumps use larger dimension to increase the flow rate, but in that case it can not be used in the lab-on-a-chip or micro-system.

5.3. THE FEATURES AND ADVANTAGES OF AC ELECTROKINETIC MICROPUMPS

Novel pumps based on ac electrokinetics are also investigated in the thesis. Here the AC electroosmosis is the main mechanism to drive fluids, which are quantitatively investigated by both experiments and FEMLAB simulations. Compared to other micropumps without moving parts, this AC electroosmotic micropump has following unique features.

(1) Low operating voltage makes it superior in terms of device portability. In our design the AC electric fields are applied to pump fluids as small as 500mV bias voltage.

(2) Avoids electrolysis and the resulting bubble generation. Currently EHD and MHD micropumps use DC fields to produce fluid motion, generating bubbles at the electrodes. In this research the applied AC fields has a frequency range of 100Hz to 5 KHz, allowing no time for bubble generation.

(3) The dimension of our micropump is 5 mm long, 500 μm wide and 100 μm height. These pumps can be scaled down linearly to submicron/nanoscale or up by expanding laterally.

(4) Minimizes pH gradient for using the smaller voltage.

(5) The designed micropump is simple in structure. The channel and electrodes array are combined to achieve electroosmotic pumping. The designed ACEO micropump can also be integrated with lab-on-a-chip for miniaturization.

These features of the AC electroosmotic pump provide higher reliability, higher compatibility and lower cost.

The designed AC electroosmotic pumps do not require open channels and hence are very useful for a sealed lab-on-a-chip system, where the fluid is circulating in closed channels. The use of this type of AC electroosmotic pump does not need open reservoir, avoiding undesired pressure due to different fluid heights in the reservoir.

5.4. Design of AC Electroosmotic Micropumps

Electroosmotic micropumps have been used widely in broad applications [52,53]. Novel micropumps based on ACEO have been designed to drive fluids. AC electroosmotic micropumps can operate at lower voltage to avoid undesirable electrolysis and pH gradients. A prototype has already been produced by Brown *et. al* [54].

The main concept of getting the pumping action is to get the uni-directional flow by breaking the reflection-symmetry in the geometry or applied signal. Fig. (5-2a) shows the pumping action breaking the symmetry by changing the geometry [55]. By using the

asymmetric pattern of electrode bigger vortices are generated on the larger electrode, which eventually dominants and produce uni-directional flow. The smaller electrode still produces the counter-rotating vortices that reduce the net flow.

Our design of AC electroosmotic micropump is based on the biased AC electroosmosis technique for symmetrical electrode array. The separation of the in-pair symmetrical electrodes (80 micron size) are 40 μm. We repeated the pair of electrodes to make the array of electrodes. The separation of the elctrode pair is 100 μm. For this particular configuration we name it 80/40/100 configuration. The corresponding numerical simulations using the finite element software FEMLAB are also conducted to verify the concept. The good agreement between the simulations and the experimental data regarding the uni-directional flow is also demonstrated.

When using the asymmetric electrode pattern the direction of the pumping can not be reversed. For several biomedical applications there is a need for bi-directional flow directions. A common medical treatment procedure makes the use of a bidirectional flow control of one or more fluids to and from a patient. For these applications we have developed the biased AC electroosmotic micropump which can operate in both directions. Here we have broken the symmetry by applying asymmetric voltage on the symmetric electrode pattern, which eventually breaks the symmetry of the pattern. Fig. 5-2(b) shows the electrode array, where L_{pair} is the separation between the two electrode pairs and L_{array} is the separation within the electrode pair. The mechanism of the designed pump is explained in Fig 5-3.

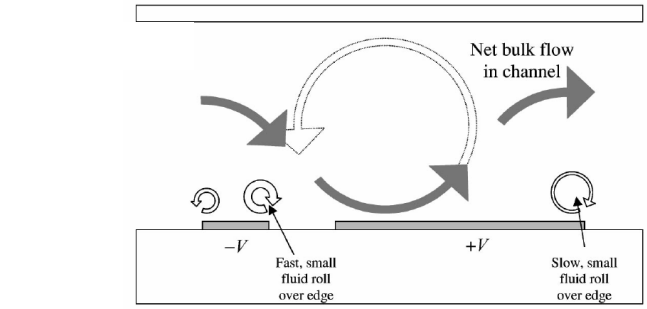

(a)

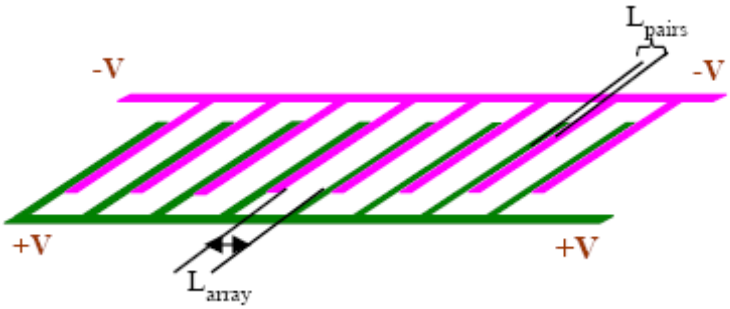

(b)

Fig. 5-2. (a) Schematic of ACEO pumping mechanism using asymmetric electrodes; (b) Proposed electrode array for ACEO pumping.

As shown in the picture, both positive biased electrode (faradic charging) and the negative biased electrode (capacitive charging) generate the same positive charges on the electrode. The electrode surface has an excess of positive charges that creates a uni-directional flow in electrode pair, which eventually produce net flow on the array of electrodes. However, the coupling between neighboring electrode pairs will produce counterflows to the net flow produced within the pair and reduce the pumping efficiency. To reduce the undesirable coupling between the two adjacent pairs, L_{array} is kept larger than L_{pair}, but not so large that the flow loses its momentum.

Fig. 5-3 is the schematic of pumping action for symmetrical electrode pattern with the biased applied voltage. The spacing L_{pair} and L_{array} will be the controlling factor for the pumping velocity. The rule of thumb is $L_{array} > L_{pair}$, so that the consecutive electrodes of L_{pair} and L_{array} do not form the EO flow in the reverse direction. From our earlier experiment we already have got L_{pair} of 20μm for the 80/20 configuration of our electrode pattern, which produces the highest fluid velocity.

Biased ACEO pump will be investigated by manipulating the faradic charging effect. We will also study the improvement in the pumping velocity. The first version of the pumping setup is shown in figure 5-4. The channel dimension is 350μm X 1.5mm X 5mm. The highest measured velocity for this pump is 150 μm/sec. The objective of the research is to increase the pumping velocity. This research also optimizes the micropumps with respect to pumping velocity for a fixed electrode geometry and applied biased AC signal [63-70].

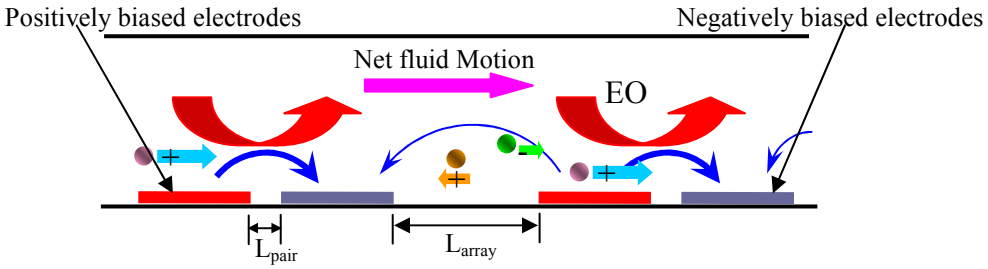

Fig. 5-3. Biased ACEO can produce uni-direction fuid motion, which also imparts differential velocities to particles with various charge/mass ratio.

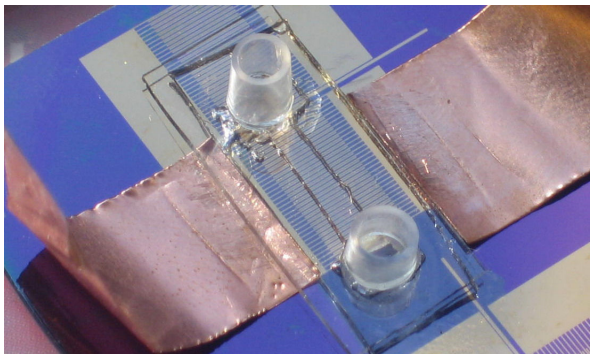

Fig. 5-4. Experimental setup of first version of the micropump.

5.5. Optimization of Micropumps

Our goal is to minimize the micropump reverse flow velocity. Obviously we increase the applied voltage it will increase the pumping velocity, and it will also increase the reverse pumping velocity (for the vortices). So, here we have focused on decreasing the reverse direction flow. Figure 5-5 explains the optimization concept by decreasing the channel height of the microfluidic chamber. Later on we also have presented the numerical simulation using FEMLAB for three different channel heights and verified the concept. The experimental result demonstrates that the thinner channel height ~ 100 μm increases the velocity of the micropump. In this case we also have demonstrated the bulk fluid flow, as here the surface to volume ratio is high.

As seen from figure 5-5, the big vortex is suppressed / obstructed by the top wall of the channel. According to our analysis the vortex size is depended on the electrode geometry and the channel height. For the fixed electrode geometry the size of the vortex is only depended on the channel height, which is explained by Comsol Multiphysics simulation in section 5.5.2. The boundary condition for inflow and outflow was the key factor to run the simuation. The boundary condition which we were is the normal inflow/outflow pressure, so that it shows the micropumping results. Our findings show that smaller channel height will increase the surface flow, which will be described more in the next section.

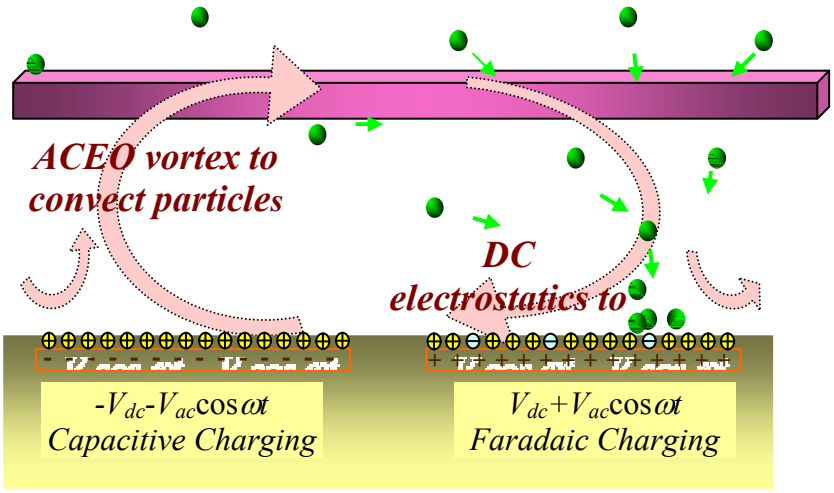

Fig. 5-5. Optimization Concept: to decrease the channel height to reduce the reverse flow.

5.5.1. Decreasing the Reverse flow of the Designed Micropump

At first in section 5.5.2, we will explain numerically regarding our motivation of decreasing the channel height for pumping optimization. If we can get the simulation result of pumping action for different channel height then we can compare the velocity field. The simulation is done with Femlab/Comsol Multiphysics package (www.comsol.com) which is discussed in section 5.5.2.

Section 5.5.3 will discuss the experimental result for the micropumping action. The main challenge is to develop the microfluidic channel for the micropump. Designing the microfluidic channel for the first version (350µm X 1.5mm X 5mm) of our micro-pump is quiet straightforward. For our first version micropump we have used the spacer coverwell (PC3L-0.5, Grace Bio-Labs, Inc.) as our microchannel. For developing the second version of the micropump (500µm X 100µm X 5mm) we have used the Si mold. The Si mold is very robust, so we get a precise 100 micron channel height.

The channel is made of transparent PDMS, so that we can analyze the fluid flow by using the tracer particles. The PDMS is cured on the mold and separate from the mold, which will give us the channel. After that, inlet and outlet is added in the system to do the pumping experiment. The inlet reservoir is filled with the particles with fluid and after applying the signal pumping action is monitored.

5.5.2. Simulation Verification of increasing Pumping velocity

Simulation of ACEO micropump has been performed prior to experiments. The simulation model, consists of two symmetrical electrodes of 80 μm width and the separation between the electrodes are 40 μm. The height of the chamber is 200 μm.

Figure 5-6 shows the normalized electric field profile from numerical simulation. The left electrode is applied with positive 1V and the right electrode is applied with negative voltage. As we can see, at the edge of the electrode the electric field is maximum. After simulating the electric field analysis we have done the Navier-Stokes simulation to calculate the velocity field in the chamber. Initial fluid velocity is set to zero for the Navier-Stokes (NS) simulation. The fluid motions are generated by applied electric signals and a large vortex is formed for biased applied signal.

Figure 5-7 compares the simulation of three different channel heights. The figure shows the streamline velocity field by Navier-Stokes. From the surface plot of the velocity field we can get the non-dimensional magnitude value of the strength of the velocity. For channel height of 250 micron (figure 5-7a) all the outer velocity streamline is completed. But as the channel height is decreased to 200 micron and 150 micron, the outer streamline velocity is cutting off. So from the pair of electrodes we can see that the velocity field increases as the channel height decreases. For doing the simulation using channel height 100 micron, does not converge in the Comsol Multiphysics.

When the array of pair of electrodes take into places, all the velocity field of the individual pair of electrodes will sum up to form a bigger vortices and form unidirectional fluid flow in the whole chamber near the surface. So for the array of

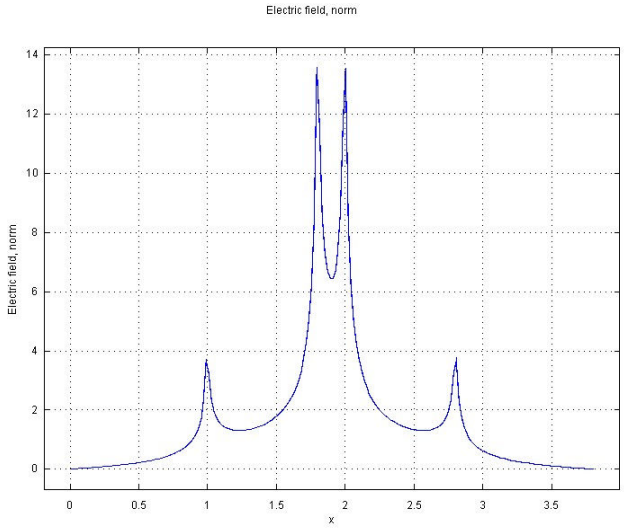

Fig. 5-6. Electric field plot for the biased AC signal on symmetrical electrode pair.

electrodes, the surface velocity will be maximized and the reverse direction flow near the top sealing of the chamber is minimized.

The non-dimensional velocity field from the simulation is shown in the Table 5-1. The position is defined as (x,y) co-ordinate in the space at the microfluidic chamber. All the y-coordinate of the data is kept smaller, so that it defines the velocity field near the surface. Our goal was to get the pumping velocity in each point on the micro-chamber, so that we can compare the different component of the fluid velocity using simulation result. We measured both the surface and the chamber velocity, which gave us an indication of the fluid velocity profile in the whole chamber. The table summarizes that, as the channel height is decreased the velocity field value is increased, i.e. the overall pumping velocity in the microfluidic chamber will increase and the pumping velocity is optimized for an applied voltage.

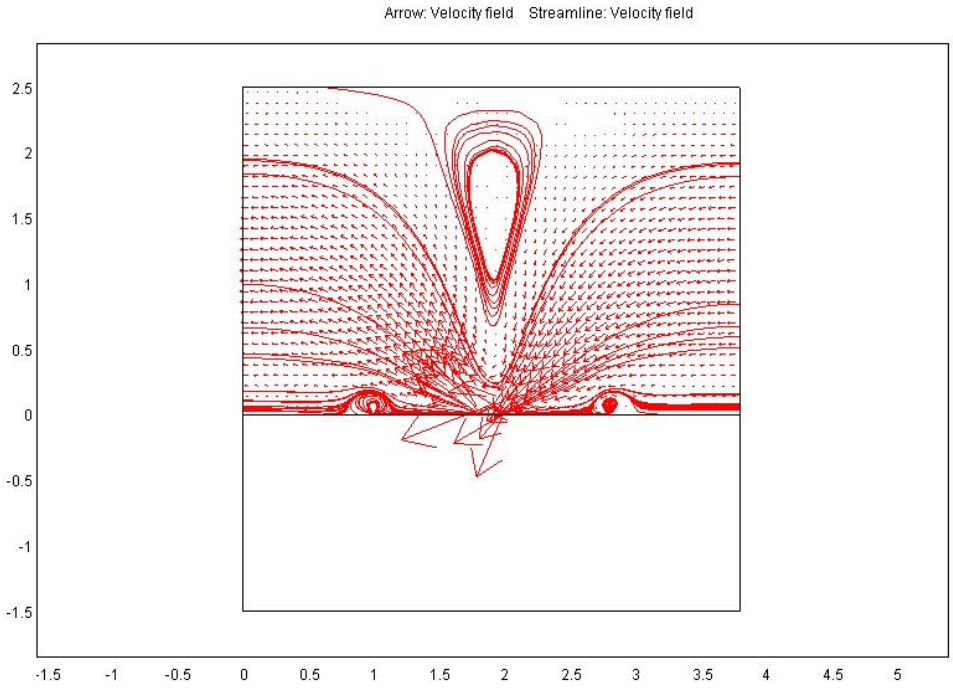
Arrow: Velocity field Streamline: Velocity field
2.5
2
1.5
1
0.5
0
-0.5
-1
-1.5
-1.5 -1 -0.5 0 0.5 1 1.5 2 2.5 3 3.5 4 4.5 5

(a)

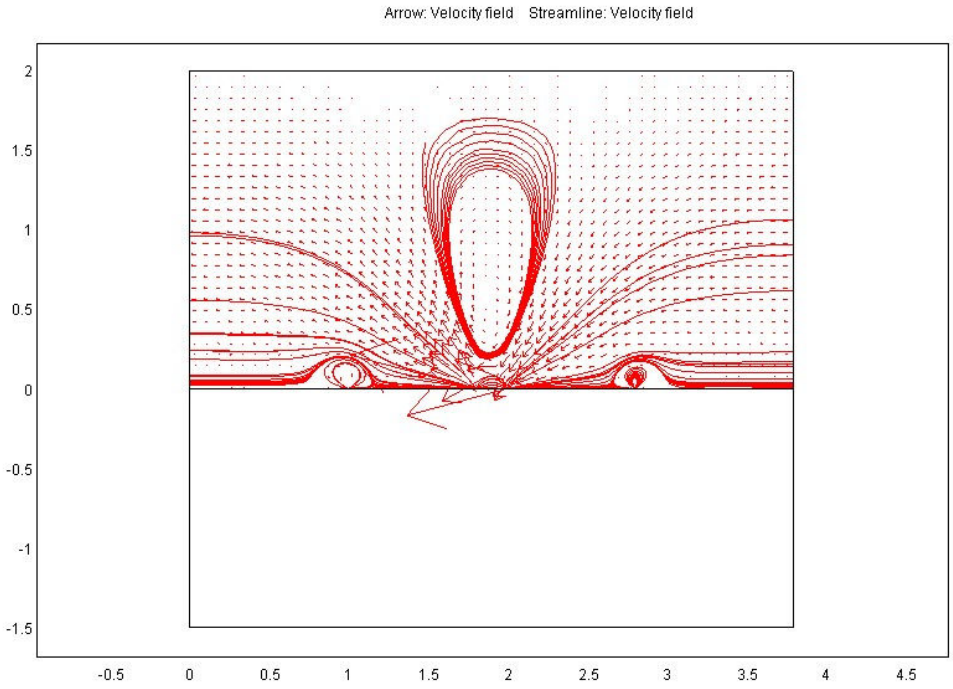
Arrow: Velocity field Streamline: Velocity field
2
1.5
1
0.5
0
-0.5
-1
-1.5
-0.5 0 0.5 1 1.5 2 2.5 3 3.5 4 4.5

(b)

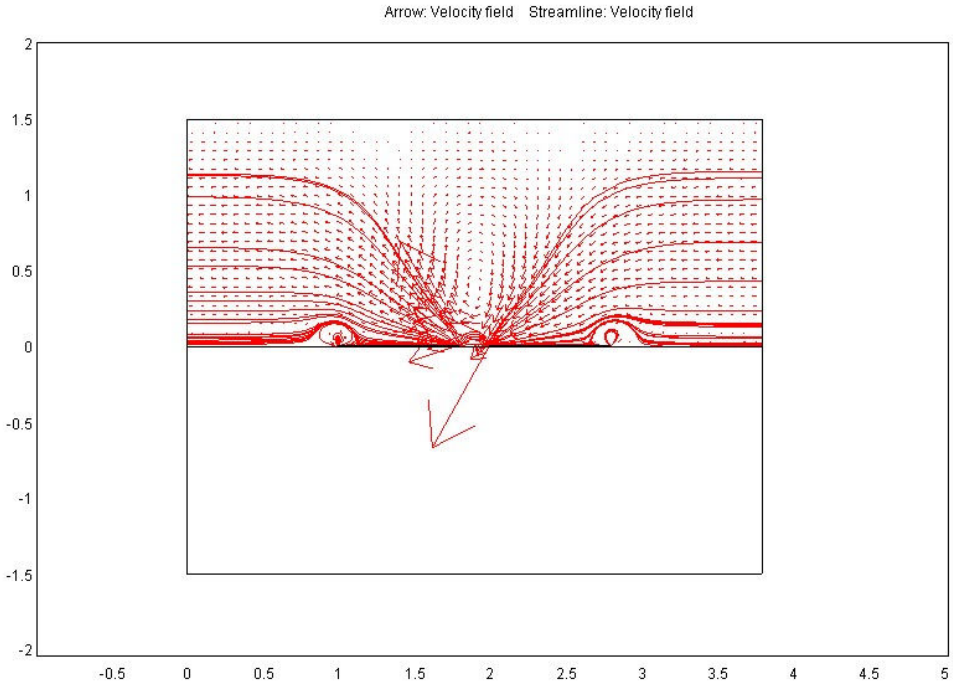

(c)

Fig. 5-7. Simulation result of biased ACEO pumping by a pair of symmetric electrodes. Streamlines are velocity field by Navier-Stokes. (a) 250 micron height Channel, (b) 200 micron height channel (c) 150 micron height channel. For smaller channel height the reverse flow is cut.

Velocity field comparison for three different channel height:

Channel Height 250 μm

Value: 2.988599, Expression: U_ns, Position: (2,0.001)
Value: 0.0003328, Expression: U_ns, Position: (2.5,0.5)
Value: 4.076119e-13, Expression: U_ns, Position: (1.4,5e-4)
Value: 4.341204e-13, Expression: U_ns, Position: (2.4,5e-4)

Height 200 μm

Value: 3.161539, Expression: U_ns, Position: (2,0.001)

Value: 0.002567, Expression: U_ns, Position: (2.5,0.5)
Value: 6.479777e-13, Expression: U_ns, Position: (1.4,5e-4)
Value: 6.265066e-13, Expression: U_ns, Position: (2.4,5e-4)

Height 150 μm

Value: 3.972204, Expression: U_ns, Position: (2,0.001)
Value: 0.002724, Expression: U_ns, Position: (2.5,0.5)
Value: 1.442087e-12, Expression: U_ns, Position: (1.4,5e-4)
Value: 1.445477e-12, Expression: U_ns, Position: (2.4,5e-4)

5.5.3. Experimental result for pumping Action

The experimental set-up of microfluidic pumping for the second version is shown in figure 5-8. As you can see from the figure the two reservoirs are at the two corners of the channel (150μm X 100μm, cross-section). The electrode array in the channel is also subdivided in two sections, so that we can do the experiments in the two individual sections or one as a whole. Initially the fluid with the tracer particle is injected in the channel using Syringe. The biased AC signal is applied through the electrode pad in the electrode array for the uni-direction pumping flow.

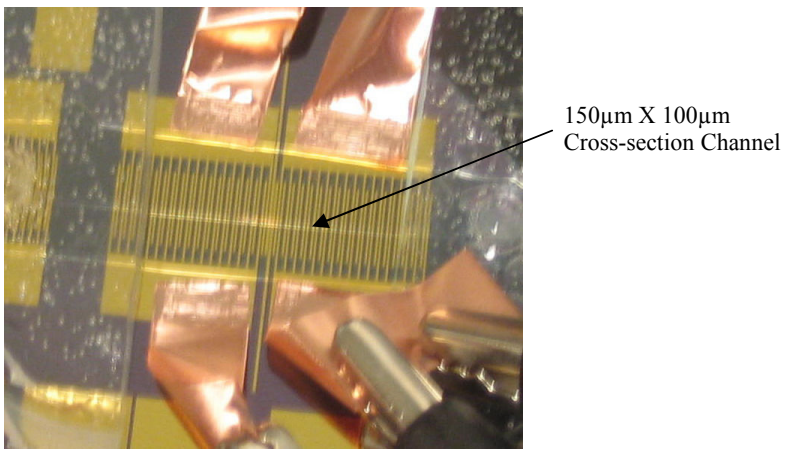

Fig. 5-8. Experimental setup of second version of the micropump.

As the cross-sectional area of the channel is on micro scale, the sealing of the channel needs to be compact. We took necessary measure to seal the whole chamber thoroughly. The interfacing of PDMS reservoir and the microchannel is done with the epoxy to seal perfectly.

Image sequence in figure 5-9 illustrates the pumping action on a particle advancing through electrode pairs. The highest measured velocity for the micropump is about 400 μm/sec, which is twice as large as the first version of the micropump. The applied AC signal has a frequency of 500Hz, with 2 V bias voltage (peak value 2V, and minimum value 0V). Increase of the bias voltage will also increase the velocity. We have also noticed the flow direction is from the positive biased electrode to the negative electrode. If we compare the different EO pumping action, we will find out that the ACEO pump the fluid with the least applied voltage.

5.5.4. Joule Heating on Electroosmotic Pumping in Microchannels

While designing AC electroosmotic pumps, the effect of fluid property variation on electroosmotic flow under the temperature variations is an important consideration. The temperature gradient in the flow channel could be attributed to Joule heating or to the thermal inequilibrium due to external factors. As a result of temperature gradient, a viscosity gradient within the channel is created and electric double layer is also influenced. Zhao *et al* [73] has developed a mathematical model to predict the electroosmotic flow under the influence of Joule heating, channel temperature variations due to other factors.

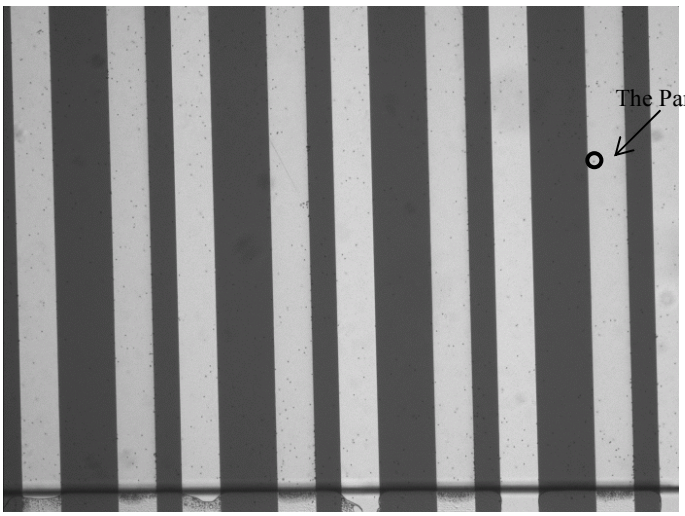

(a)

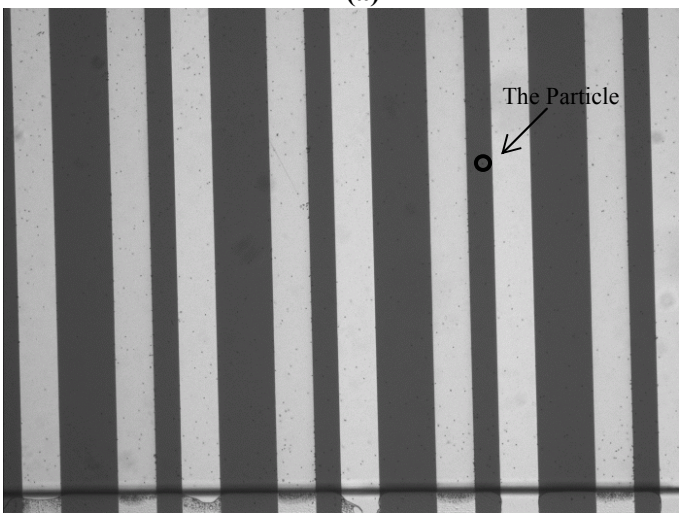

(b)

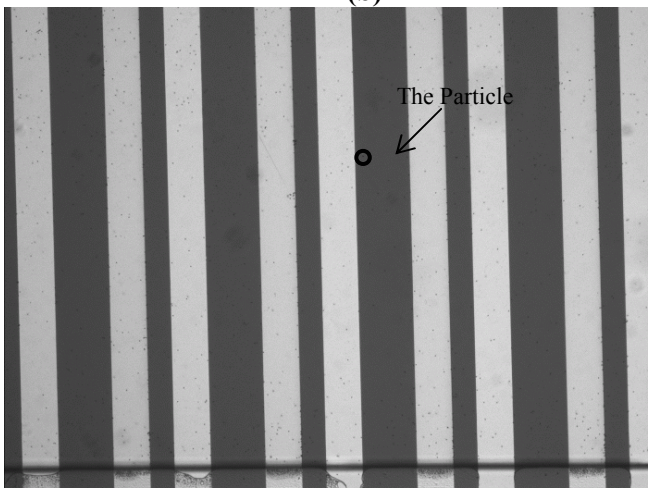

(c)

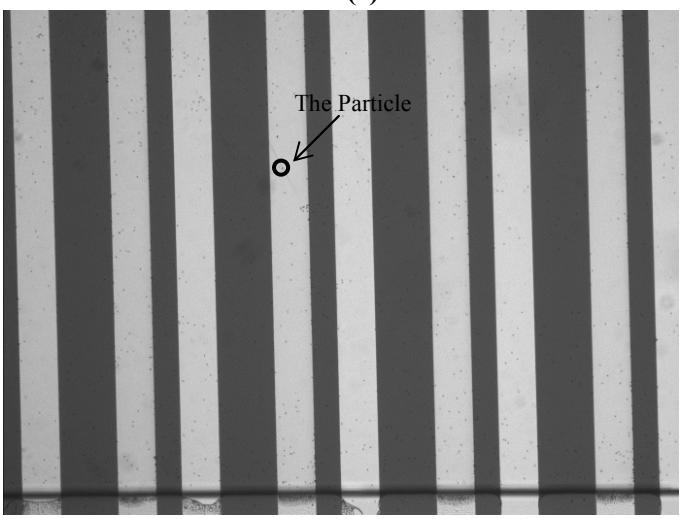

(d)

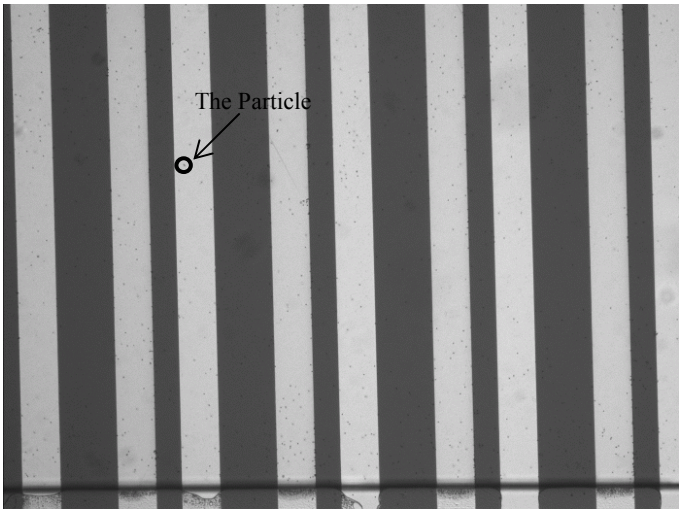

(e)

Fig. 5-9. Image sequence of the particle advancing through the array of electrodes. The focal plane of the image is about 5 μm above the wafer surface in a 100μm deep channel. The bright areas are electrodes and dark areas are insulators. (a) t = 0s, (b) t = 1.5s, (c) t = 3s, (d) t = 4.5s, (e) t = 6s.

To take into account the Joule heating we have measured the pumping current for the applied AC voltage. For significant Joule heating, the pump performance can vary substantially as compared to models that do not take temperature variations into account. Figure 5-10 and 5-11 shows the pumping current and pumping velocity with respect to the applied AC signal. As you can see from the figure 5-10, the maximum current is 0.012 mA. Now, Joule heating, $P = i^2R$. So the square of the maximum current will be smaller and will give a smaller value of P. From figure 3-6, the maximum impedance is 12 KΩ. By using this value and 0.012 mA current, we get P = 1.73 micro Watt. Thus we can neglect the heating in our pumping action. As the AC-EO micropump is pumping the liquid, so we can neglect the heating effect in the microchannel. But the current and velocity plot (Figure 5-10 and 5-11) will be very useful for the control circuit of the micropump. The more of the feedback (F/B) circuit and controlling the micropump action will be discussed in the future work section.

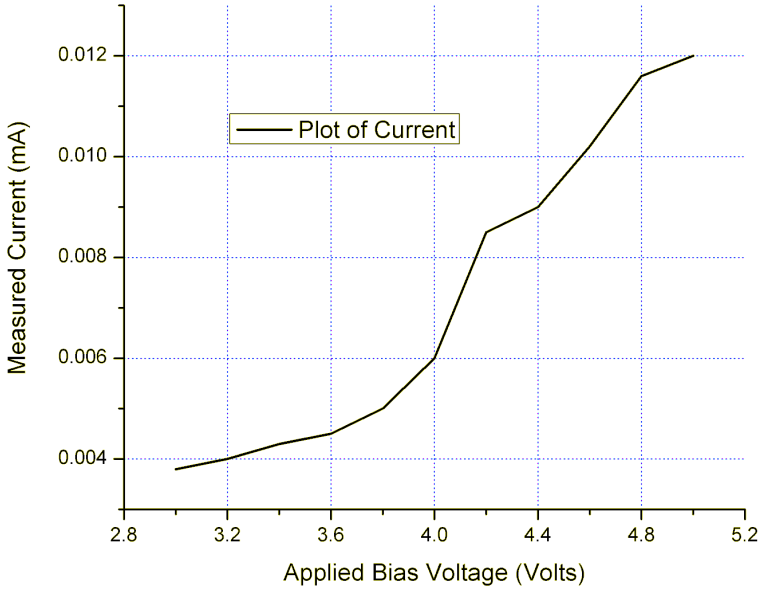

Fig. 5-10. Experimental result of measured current for the micropump.

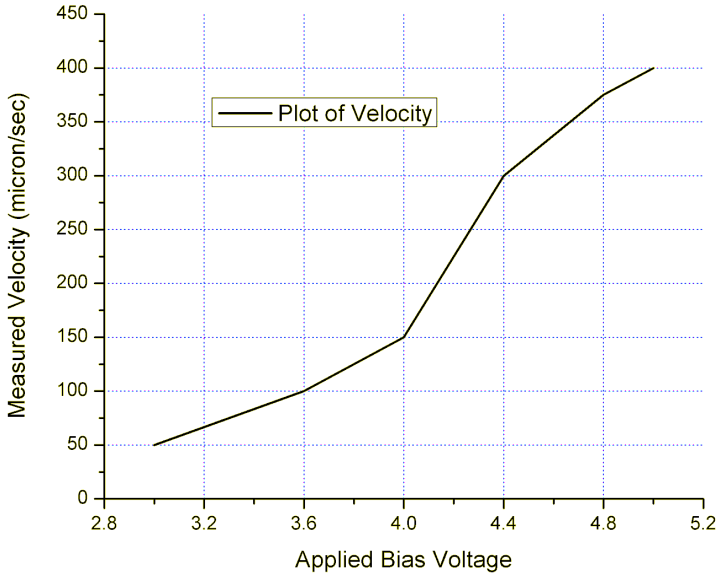

Fig. 5-11. Experimental result of measured velocity for the micropump.

CHAPTER 6. CONCLUSION AND FUTURE WORK

A novel technique has been developed to trap the particles and pump the fluid. Interfacing the micro-cantilever with ACEO mechanism has expanded its capability for biological, physical and chemical detection and makes the whole system ultra sensitive. The research work substantially enriches the portfolio of transducers that can be used in high performance miniaturized analytical systems.

Some important applications of ACEO designs are in the fields of diagnostics and biosensors. For example, concentrating bacteria from a dilute solution is an important challenge in the biomedical research. Dielectrophoresis force, which has been suggested as a way of trapping these organisms, decays at a much shorter distance than AC electroosmotic flow. AC electroosmotic flow is a promising way to concentrate bioparticles and assemble them near the sensors. Several groups have exploited combined DEP and EHD effects to trap particles or bacteria from solution onto the top of electrode surfaces in the recent years [32, 33].

AC electroosmosis, with its advantages of low power, low voltage and higher velocity, has been used to develop pumps. Such an AC electrokinetic micropump is presented by Olesen [31] which has fast pumping (velocities » mm/s) velocity with low driving voltage of a few volts. But he has used the asymmetric pattern of electrodes. This thesis also presents the novel micropump which utilizes the symmetric electrode pattern with the bias AC voltage.

The novel DC-biased, AC electroosmotic micropump operates in low voltage to avoid undesirable electrolysis and pH gradients. The developed uni-directional micropump prototype breaks the symmetry of the electrode array by applying the DC-biased AC signal, which has proven to be advantageous when compared to those pumps that use only asymmetric electrode patterning.

6.1. RELEVANT PUBLICATIONS

The following is a list of publications covering to contributions made thus far, as described in this work:

[1] N. Islam, M Lian, and J. Wu, "Enhancing Microcantilever Sensitivity with Integrated AC Electroosmotic Trapping," Journal of Microfluidics and Nanofluidics, accepted for publication.

[2] J. Wu and N. Islam, "A Simple Method to Integrate in-situ Nano-Particle Focusing with Cantilever Detection," IEEE Sensors Letters, accepted for publication.

[3] N. Islam and J. Wu, "Microfluidic Transport by AC Electroosmosis", Journal of Physics: Conference Series, 34, pp. 356 – 361, 2006

[4] M. Lian, Nazmul Islam and J. Wu, "Particle Line Assembly/Patterning by Microfluidic AC electroosmosis," Int'l MEMS Conf., May 9-12, 2006, Singapore, J. Phys.: Conf. Series, 34, pp. 589 – 594, 2006

[5] M. Lian, N. Islam, and J. Wu, "AC electrothermal effect on particle manipulation and pumping." Submitted to Journal of IET Nanobiotechnology.

[6] N. Islam, M. Lian, J. Wu, R. Zhou, P. Wang and H.-C. Chang, "Bio/nano- particle Capture, Concentration and Detection by AC Electrokinetics," ORNL CNMS 2006 User Meeting, June 14-16, 2006, Oak Ridge, TN. (Invited Poster)

[7] J. Wu, N. Islam and M. Lian, "High Sensitivity Particle Detection By Biased AC Electro-Osmotic Trapping on Cantilever," 19th IEEE Int'l Conf. Micro Electro Mechanical Systems (MEMS 2006), Jan. 22-26, 2006, Istanbul, Turkey, in press.

[8] N. Islam, M. Lian, S. Swaminathan and J. Wu, "Micro/Nano- Particulate Fluid Manipulation in AC Electro-Kinetic Lab-on-a-Chip," 2nd ASM - IEEE EMBS Conf. Bio, Micro & Nanosyst., Jan. 15-18, 2006, San Francisco, CA, USA.

[9] N. Islam, and J. Wu, "AC Electro-osmotic Micropump using Asymmetric Polarization", ASME NanoMechanics: Sensors & Actuators, May 16 –18 2005, Knoxville, TN

6.2. FUTURE WORK

Developing the feedback system of micro-pumping action for the biased ACEO can be a potential future task. The performance and reliability of a micropump is dependent on its feedback compensation, which maximises or minimises the performance criteria that is unknown until the completion of the optimising process. Figure 6-1 illustrates a simple adaptive control system for a micropump of varying current that are continuously measured and then compensated so that the system performance criteria are always satisfied.

The level of current from the micropump is proportional to the velocity of the micropump (Fig. 5-10 and 5-11). The micropump current is collected (integrated) on the feedback capacitor of the integrator (Fig. 6-1). The switched capacitor integrator presents a low impedance to the micropump and sets the detector bias voltage. The rate at which the output voltage of the integrator increases is directly proportional to the level of

current from the micropump. As an integrator we used an Operational Transconductance Amplifier (OTA) in our circuit.

As the output voltage of the integrator (OTA) is proportional to photocurrent, V_{out} continues to increase until it reaches a level, V_{ref}, equal to the reference voltage of the comparator. The offset voltage for a comparator is the differential voltage at the input. Ideally this should be zero, so that the output transition occurs exactly when the integrator output reaches the threshold voltage. When this level (V_{ref}) is reached the output of the comparator changes from low to high. This transition triggers a pulse at the output of a monostable multivibrator (one-shot). So the output high from the comparator will not let the voltage to increase and the feedback loop will control the applied voltage.

It can be demonstrated by this work that it is possible to produce an adaptive closed-loop system model based on the characterization of a micropump. For the improvement of microfabrication technology the whole feedback control unit can be integrated with the micropump. This will take the lab-on-a-chip (LOC) application to a new direction.

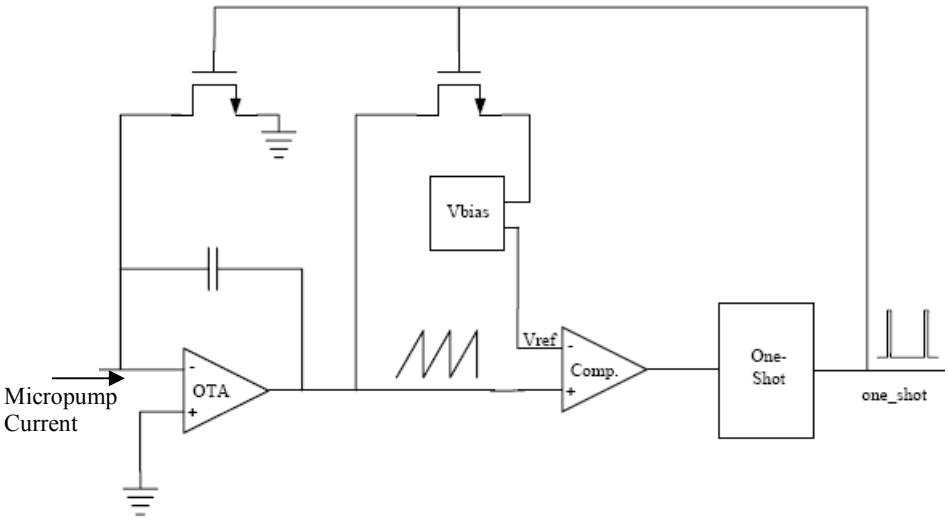

Fig. 12-13. Feedback Control of the Micropump

REFERENCES

[1] Helene Andersson, Albert ven den Berg, " Microfluidic devices for cellomics : A review", Sensors and Actuators, B 92, (2003), 315-325.

[2] Vincent Studer, Anne Pépin, Yong Chen, and Armand Ajdari, "An integrated ac electrokinetic pump in a microfluidic loop for fast and tunable flow control", Analyst, vol. 129, pp. 944-949, 2004.

[3] C.-H. Chen and J.G. Santiago, "A planar electroosmotic micropump," J. Microelectromech. Syst., vol. 11, pp. 672-683, 2002.

[4] Lastochkin, D., Zhou, R., Wang, P., Ben, Y. and Chang, H.-C., "Electrokinetic Micropump and Micromixer Design Based on AC Faradaic Polarization", J. of Applied Physics , 96 , 1730 (2004).

[5] K. H. Bhatt, S. Grego and O. D. Velev, "An AC Electrokinetic Technique for Collection and Concentration of Particles and Cells on Patterned Electrodes," *Langmuir* **21**, pp. 6603-6612, 2005.

[6] M. R. Brown, and C. D. Meinhart, "AC electroosmotic flow in a DNA concentrator," Microfluidics & Nanofluidics, ISSN:1613-4982 (Print) 1613-4990 (Online), 2006.

[7] Ronald F. Probstein, Physicochemical Hydrodynamics : An Introduction, 2nd Editon, New York : John Wiley and Sons, c 1994

[8] Stone, H.A. and S. Kim, "Microfluidics: Basic issues, applications, and challenges," AIChE J., 47(6), 1250-1253 (2001).

[9] A. Ramos, H. Morgan, N. G. Green and A. Castellanos, "AC electrokinetics: a review of forces in microelectrode structures", J. Phys. D: Appl. Phys. 31(1998) 2338–53

[10] A. Ramos, H. Morgan, N. G. Green and A. Castellanos, "AC electric-field-induced fluid flow in microelectrodes", J. Colloid Interface Sci. 217(1999) 420–2

[11] J. Wu, "Electrokinetic Microfluidics for On-Chip Bioparticle Processing," IEEE Trans. Nanotech., Mar. 2006.

[12] J. Wu, Y. Ben and H.-C. Chang, "Particle Detection by Micro- Electrical Impedance Spectroscopy with Asymmetric-Polarization AC Electroosmotic Trapping," Microfluidics & Nanofluidics, 1(2), pp. 161-167, 2005

[13] Julio M. Ottino and Stephen Wiggins, " Introduction: mixing in microfluidics", Phil. Trans. Royal Society Lond. A (2004) 362, 923-935.

[14] N. Islam, M. Lian, S. Swaminathan and J. Wu, "Micro/Nano- Particulate Fluid Manipulation in AC Electro-Kinetic Lab-on-a-Chip," 2nd ASM - IEEE EMBS Conf. Bio, Micro & Nanosyst., Jan. 15-18, 2006, San Francisco, CA, USA.

[15] J. Wu, N. Islam and M. Lian, "High Sensitivity Particle Detection By Biased AC Electro-Osmotic Trapping on Cantilever," 19th IEEE Int'l Conf. Micro Electro Mechanical Systems (MEMS 2006), Jan. 22-26, 2006, pp. 566 – 569, Istanbul, Turkey.

[16] N. Islam, M Lian, and J. Wu, "Enhancing Microcantilever Sensitivity with Integrated AC Electroosmotic Trapping," submitted to Bio-microfluidics Journal.

[17] J. Wu and H.-C. Chang, "Asymmetrically Biased AC Electrochemical Micropump," AIChE annual meeting 2004, Nov. 7 – 12, Austin, TX.

[18] Rosenthal A, Voldman J, "Dielectrophoretic traps for single-particle patterning," Biophysical Journal, 88(3), pp. 2193-2205, 2005.

[19] Meinhart C D, Wang D and Turner K, "Measurement of AC Electrokinetic Flows," J. Biomedical Microdevices, 5(2), 139-145, 2003

[20] Morgan H, Green N G, “Electrokinetics: Colloids and Nanoparticles,” Research Studies Press Ltd: UK 2002

[21] Sepaniak M, Datskos P, Lavrik N, Tipple C, “Microcantilever Transducers: A New Approach in Sensor Technology,” Analytical Chemistry, November 1, pp. 568A-575A, 2002.

[22] Green N G, Ramos A, Gonzalez A, Morgan H, and Castellanos A, “Fluid flow induced by nonuniform ac electric fields in electrolytes on microelectrodes. III. Observation of streamlines and numerical simulation,” Physical Review E 66, 026305, 2002.

[23] Taylor, M. T., “ Simulation of microfluidic pumping in a genomic DNA blood-processing cassette,” Journal of Micromechanics and Microengineering, 2003. 13(2): pp 201-208.

[24] Laser, D. and J. Santiago, “A Review of micropumps,” J. Micromechanics and Microengineering, 2004. 14:pp R34-R64.

[25] T.M. Squires and M.Z. Bazant, “Induced-charge Electro-osmosis,” J. Fluid Mech., 509, pp. 217-252, 2004.

[26] Vincent Studer, Anne Pépin, Yong Chen, and Armand Ajdari, “An integrated ac electrokinetic pump in a microfluidic loop for fast and tunable flow control”, The Analyst Journal, 129, 944-949, 2004.

[27] Lastochkin, D., Zhou, R., Wang, P., Ben, Y. and Chang, H.-C., "Electrokinetic Micropump and Micromixer Design Based on AC Faradaic Polarization", J. of Applied Physics , 96 , 1730 (2004).

[28] Iki, N., H. Hoshino, and T. Yotsuyanagi, “ A capillary electrophoretic reactor with an electroosmosis control method for measurement of dissociation kinetics of metal complexes,” Analytical Chemistry, 2000. 72(20): pp. 4812-4820.

[29] J. Wu, N. Islam and M. Lian, "High Sensitivity Particle Detection By Biased AC Electro-Osmotic Trapping on Cantilever," 19th IEEE Int'l Conf. Micro Electro Mechanical Systems (MEMS 2006), Jan. 22-26, 2006, pp. 566 – 569, Istanbul, Turkey.

[30] M. Z. Bazant, T. M. Squires, "Induced-charge Electrokinetic Phenomena: Theory and Microfluidic Applications", Phys. Rev. Letter, 92(6), 066101 (2004)

[31] L. Olesen, H. Bruus, A Ajdari, "AC electrokinetic micropumps: the effect of geometrical confinement Faradaic current injection, and nonlinear surface capacitance", Phys. Rev. E, **73**, 056313 (2006).

[32] P.K. Wong, C. Y. Chen, T. H. Wang and C. M. Ho, "An AC Electroosmotic Processor for Biomolecules"' Transducers 03 the 12th International Conference on Solid-State, Sensors Actuators and Microsystems, 1, 20 (2003)

[33] K. F. Hoettges, M. B. McDonnell and M. P. Hughes, "Use of Combined Dielectrophoretic/Electrohydrodynamic Forces for Biosensor Enhancement", J. Physics D: Appl. Physiscs, 36, L101 (2003)

[34] A. Castellanos, A. Ramos, A. Gonzalez, N. G. Green, and H. Morgan, "Electrohydrodynamics and dielectrophoresis in microsystems: Scaling laws," J. Phys. D, Appl. Phys., vol. 36, pp. 2584–2597, 2003.

[35] D. Ivnitski, I. Abdel-Hamid, P. Atanasov, and E. Wilkins, "Biosensors for detection of pathogenic bacteria," Biosens. Bioelectron., vol. 14, pp. 599–624, 1999.

[36] J. Suehiro, M. Shutou, T. Hatano and M. Hara, "High sensitive detection of biological cells using dielectrophoretic impedance measurement method combined with electro-permeabilization," Sensor and Actuator B, Vol. 96, pp. 144–151, 2003.

[37] Josh H. M. Lam, Raymond H. W. Lam, Kin Fong Lei, Winnie W. Y. Chow and Wen J. Li, "A Polymer-based Micro fluidic Mixing System Driven by Vortex Micropumps", Proceedings of the 5th World Congress on Intelligent Control and Automation, June 15-19, 2004.

[38] M. Mpholo, C. G. Smith, A. B. D. Brown, "Low voltage plug flow pumping using anisotropic electrode arrays", Sensors and Actuators B 92 (2003) 262-268.

[39] C. Liu, D. Cui, H. Cai, X. Chen, Z. Geng, "A rigid poly(dimethylsiloxane) sandwich electrophoresis microchip based on thin-casting method", Electrophoresis 2006, 27, 2917–2923

[40] M.Kanaip, D.Uchida, S.Sugiura, Y.Shirasaki, J.S.Go, H.Nakanishi, T.Funatsu and S.Shoji, " PDMS microfluidic devices with PTFE passivated channels", 7th lnternational Conference on Miniaturized Chemical and Biochemical Analysts Systems October 5-9, 2003, California USA

[41] Z. Wu, H. Jensen, J. Gamby, X. Bai and H. H. Girault, "A flexible sample introduction method for polymer microfluidic chips using a push/pull pressure pump", Lab on a Chip Journal, 2004 , 4, 512–515

[42] Gonzalez A, Green N G, Ramos A, Morgan H, and Castellanos A, "Fluid flow induced by nonuniform ac electric fields in electrolytes on microelectrodes. II. A linear double-layer analysis," Physical Review E 61(4),pp 4019-4028 , April, 2000.

[43] M. Sigurdson, D. Wang and C. D. Meinhart, " Electrothermal stirring for heterogeneous immunoassays",Lab on a Chip Journal, 2005, 5, 1366–1373

[44] N.G. Green, A. Ramos, A. Gonzalez, A. Castellanos, and H. Morgan, "Electrothermally induced fluid flow on microelectrodes," Journal of Electrostatics, 53 (2001) 71-87.

[45] Vincent Studer, Anne Pépin, Yong Chen, and Armand Ajdari, “An integrated ac electrokinetic pump in a microfluidic loop for fast and tunable flow control”, The Analyst Journal, 129, 944-949, 2004.

[46] D. J. Laser and J. G. Santiago, “A review of micropumps”, Journal of Micromechanics and Microengineering, Institute of Physics Publishing 14 (2004), R35-R64.

[47] Krutzch W C and Cooper P 2001 Introduction: classification and selection of pumps Pump Handbook ed I J Karassik et al (New York: McGraw-Hill)

[48] Nam-Trung Nguyen, Xiaoyang Huang, and Toh Kok Chuan, “MEMS-Micropumps: A Review”, ASME, Vol.124, June 2002.

[49] Zilin Chen, Ping Wang, and Hsueh-Chia Chang, “An electro-osmotic micro-pump based on monolithic silica for micro-flow analyses and electro-sprays”, Anal Bioanal Chem (2005) 382, 817-824.

[50] Shulin Zeng et al., “Fabrication and characterization of electroosmotic micropumps”, ELSEVIER-Sensors and Actuators B79 (2001), 107-114.

[51] Shulin Zeng et al., “Fabrication and Characterization of Electrokinetic Micropumps”, Inter Society Conference on Thermal Phenomena 2000.

[52] Lastochkin, D., Zhou, R., Wang, P., Ben, Y. and Chang, H.-C., "Electrokinetic Micropump and Micromixer Design Based on AC Faradaic Polarization", J. of Applied Physics , 96 , 1730 (2004).

[53] Iki, N., H. Hoshino, and T. Yotsuyanagi, “ A capillary electrophoretic reactor with an electroosmosis control method for measurement of dissociation kinetics of metal complexes,” Analytical Chemistry, 2000. 72(20): pp. 4812-4820.

[54] M. Mpholo, C. G. Smith, A. B. D. Brown, “Low voltage plug flow pumping using anisotropic electrode arrays”, Sensors and Actuators B 92 (2003) 262-268.

[55] A. Ramos, A. Gonzalez, A. Castellanos, N.G. Green, and H. Morgan, “Pumping of liquids with ac voltages applied to asymmetric pairs of microelectrodes,” Phys. Rev. E, 67, 056302 (2003).

[56] Shaorong Liu, Qiaosheng Pu, and Joann J. Lu, “Electric field-decoupled electroosmotic pump for microfluidic devices”, Journal of Chromatography A, 1013 (2003), 57-64.

[57] Ping Wang, Zilin Chen, and Hsueh-Chia Chang, “A new electro-osmotic pump based on silica monoliths”, ELSEVIER-Sensors and Actuators B113 (2006), 500-509.

[58] A. Ramos, H. Morgan, N. G. Green, A. Castellanos. “AC electrokinetics: a review of forces in microelectrode structures”. J. Phys. D: Appl. Phys. Vol 31. pp 2338-2353.

[59] N.G. Green, A. Ramos, A. Gonzalez, H. Morgan, and A. Castellanos, “Fluid flow induced by nonuniform ac electric fields in electrolytes on microelectrodes. III. Observation of streamlines and numerical simulation,” Physical Review E, 2002, Vol.66, 026305

[60] Shuhuai Yao and Juan G. Santiago, “Porous glass electroosmotic pumps: theory”, ELSEVIER- Journal of Colloid and Interface Science, 268 (2003), 133-142.

[61] Chuan-Hua Chen and Juan G. Santiago, “A Planar Electroosmotic Micropump”, Journal of Microelectromechanical Systems, Vol.11, No.6, December 2002.

[62] J.-G. Choi, M. Kim, R. Dadoo, and R.N. Zare, “Electrophoretron: a new method for enhancing resolution in electrokinetic separations,” J. Chromatogr., vol. 924, pp. 53-58, 2001.

[63] N. Burggraf, A. Manz, E Verpoorte, C.S. Effenhauser, H.M. Widmer, and N.F. de Rooij, “A novel approach to ion separations in solution: synchronized cyclic capillary electrophoresis (SCCE),” Sens. Actuators B, Vol. 20, pp. 103-110, 1994.

[64] J. Darabi, M. Rada, M.M. Ohadi, and J. Lawler, “Design, Fabrication, and testing of an Electrohydrodynamic Ion-drag micropump,” J. Microelectromech. Syst., Vol. 11, pp. 684-690, 2002.

[65] C.-H. Chen and J.G. Santiago, “A planar electroosmotic micropump,” J. Micro Electro Mech. Syst., vol. 11, pp. 672-683, 2002.

[66] A.R. Minerick, A.E. Ostafin, H.-C. Chang, “Electrokinetic transport of red blood cells in micocapillaries,” Electrophoresis, vol. 23, pp. 2165-2173, 2002.

[67] M. Trau, D. A. Saville, I. A. Aksay, “Field-Induced Layering of Colloidal Crystals,” Science, 272, 706 (1996).

[68] S. R. Yeh, M. Seul, B. I. Shraiman, “Assembly of ordered colloidal aggregates by electric-field-induced fluid flow,” Nature, 386, 57 (1997).

[69] P.K. Wong, C.-Y. Chen, T.-H. Wang and C.-M. Ho, "An AC Electroosmotic Processor for Biomolecules", TRANSDUCERS’ 03, 8-12 June 2003, pp. 20-23.

[70] K.F. Hoettges, M.B. McDonnel and M.P. Hughes, “Use of combined dielectrophoretic/ electrohydrodynamic forces for biosensor enhancement,” J. Phys. D; Appl. Phys. Vol. 36, pp. L101-104, 2003.

[71] P. H. Paul, D.W. Arnold, and D. J. Rakestraw, “Electrokinetic generation of high pressures using porous microstructures,” in _-TAS 98, Banff, Canada, 1998.

[72] S. Zeng, C. H. Chen, J. C. Mikkelsen Jr., and J. G. Santiago, “Fabrication and characterization of electroosmotic micropumps,” Sensors Actuat. B, vol. 79, pp. 107–114, 2001

[73] T S Zhao and Q Liao," Thermal effects on electro-osmotic pumping of liquids in microchannels", T S Zhao et al 2002 J. Micromech. Microeng. 12 962-970 doi:10.1088/0960-1317/12/6/329

[74] Nazmul Islam, Syed K. Islam, Stephen C. Terry, Mo Zhang and Benjamin Balock, "Low Power Bioluminescent Bioreporter Integrated Circuit (BBIC) for Photodetection", 13th Annual Symposium on Microelectronics and Optoelectronics, Connecticut, April 7, 2004, Storrs, CT.

[75] Davis, C, Booth, D, J, Harvey, E, Cadusch, P, Mazzolini, A and Askraba S, "Dynamic measurements of a micropump using a fibre based interferometer", Centre for Imaging and Applied Optics, Swinburne University of Technology, Victoria, 3122, Australia (1999).

[76] A. Ramos, A. Gonzalez, A. Castellanos, N.G. Green, and H. Morgan, "Pumping of liquids with ac voltages applied to asymmetric pairs of microelectrodes," Phys. Rev. E, 67, 056302 (2003).

[77] N. Islam and J. Wu, "Microfluidic Transport by AC Electroosmosis", Journal of Physics: Conference Series, 34, pp. 356 – 361, 2006

VITA

Nazmul Islam received the B.S degrees in Electrical Engineering from Bangladesh University of Engineering & Technology (BUET), Dhaka, Bangladesh in 1999. After that he finished his M.Sc in Electrical Engineering from Virginia Polytechnic Institute and State University (Virginia Tech) in August 2002. Currently, he is working on the doctoral research works in the department of Electrical & Computer Engineering of the University of Tennessee, Knoxville and expected to be graduated in May 2007. His major research interest concentrates in the areas of Microfluidics, Solid- State sensors and Actuators, and Nanosystems. He also has the knowledge and expertise of IC design flow from schematic to pad-to-pad simulation using the CAD tools cadence for both analog and digital design. He has a good academic background and received Bangladesh Government Merit Scholarship (1985-1990), BUET Talent Scholarship (1994-1999), teaching assistantship (2000-2002). He is currently Research Assistant at the Electromechanics and Transducer research group in Electrical and Computer Engineering department at the University of Tennessee.